Ti-Fe Binary Oxides Nanomaterial's: Synthesis, Characterization, Adsorption and Photocatalytic Activity

By
Buzuayehu Abebe (MSc)
Yilkal Dessie (MSc)

A Project submitted to
Office of Research Project Management
Adama Science and Technology University

Adama, Ethiopia
December, 2019

List of Tables

List of Figures

List of Abbreviations

ROS	Reactive oxidative species
AOP	Advanced oxidation process
XRD	X-ray diffraction
FT-IR	Fourier transform infra-red
SEM	Scanning electron microscopy
EDX	Energy-dispersive X-ray
TGA-DTA	Thermogravimetric - differentialthermal analysis
BET	Brunauer–Emmett–Teller
D-RK	Dubinin-Radushkevich
FG	Fowler-Guggenheim
FH	Flory-Huggins
PFO	Pseudo-first-order
PSO	Pseudo-first-order
IPD	Intra-particle adsorption-diffusion
L-H	Langmuir–Hinshelwood
MO	Methyl orange

Acknowledgments

Authors are great full to the management of Adama Science and Technology University for providing financial support. Author's also great full to Dr. H C Ananda Murthy for characterization of samples in India as well as for his continuous assistance throughout the work. Author's also needs to forward deep acknowledgement to Dr. Dereje Tsegaye for his write up improvement and Mr. Guta Amanu for his assistance in the laboratory. Finally, the authors need to acknowledge Fikadu Tsegaye his assistance on conducting the adsorption and photocatalysis test in Haramaya University.

Table of Contents

Abstract

Water pollution is the most serious problems in the environmental fields. Organic solvent free impregnation method was used to synthesize titanium-iron oxides (TIOs) nanomaterial for the degradation of methyl orange dye. The physical properties of synthesized TIOs photocatalyst materials were characterized by XRD, SEM-EDX, BET, UV-Vis, and FT-IR analytical techniques. The appearance of iron oxide (α-Fe_2O_3) on SEM image, XRD, and EDX spectra; the redshift on UV-Vis spectra of TIO compared to titanium oxide (TiO_2); and intensity reduction on FT-IR spectra proves the good impregnation of α-Fe_2O_3 in TiO_2 lattice. The Langmuir and Dubinin-Radushkevich (D-RK) adsorption isotherm test in the dark show the domination of physical adsorption. Furthermore, the Flory-Huggins (FH) isotherm model that has ΔG = -11.40 kJ/mol confirm the spontaneity of the reaction. The passing of the linear Weber–Morris intra-particle adsorption-diffusion (IPD) plot through the origin and well-fitting of its coefficient of determination (R^2) value relative to pseudo-first-order (PFO) indicates the domination of adsorption-diffusion mechanism. On the methyl orange (MO) degradation experiment, as the percentage of Fe_2O_3 increases from 4 to 12, its degradation efficiency decrease, i.e. TIO with 4 % calcined at 500 ^oC (TIO-4) has higher degradation efficiency with k values of 0.03025. The TIOs binary oxides containing a different percentage of α-Fe_2O_3 were also used for lead ion removal. During adsorption study pH of the solution, adsorbent dosage, time of contact, agitation speed, and concentration of adsorbate were optimized. From Langmuir, Freundlich, FG, D-RK, Temkin, FH adsorption isotherm models, relatively, the Langmuir isotherm model fits well. For adsorption-reaction kinetics model pseudo first order (PFO), pseudo-second order (PSO) and Elovich was tasted and intraparticle diffusion (IPD) for adsorption-diffusion kinetics models. Out of those the PSO fits well, this indicates that the mechanism of adsorption is under control of adsorption-reaction. The mean adsorption energy, reproducibility of the adsorbent was also conducted and all of those studies support the domination of physical adsorption mechanism. Furthermore, the spontaneity of the reaction test also accomplished.

Keywords: *Binary Ti-Fe oxides; Lead ion; Methyl orange; adsorption isotherms, kinetics, and thermodynamics*.

1. Introduction

Nowadays, water pollution has become one of the most serious problems in the environmental fields. Therefore, with the rapid development of industrial society, increasing environmental-safety threats pose a major concern (Ali et al. 2018; Basheer 2018). Among numerous physicochemical methods used for pollutant remediation including adsorption (Abebe and Ananda Murthy 2018), flocculation (Gallego-Urrea et al. 2016), coagulation (Tang et al. 2016), molecular sieves (Wang et al. 2017), ion exchange (Charles et al. 2016), and reverse osmosis (Pype et al. 2016), the adsorption combined with advanced oxidation processes (heterogeneous photocatalysis) using semiconductor metal oxides has gained more attention in the scientific community (Chen et al. 2017).

It's known that, semiconductor metal oxides are widely used for adsorption of toxic metal ions and degradation of different dyes from aqueous solution. Among numerous metal oxide photocatalyst, TiO_2 is known for its strong oxidizing power, good stability, and environmental compatibility. However, because of its high bandgap energy (~3.2 eV), low surface area to volume ratio and rapid electron-hole (e^--h^+) recombination properties, the photocatalytic effectiveness and adsorption capacity of bare TiO_2 is quite less (Wu et al. 2017). In order to reduce these drawbacks and to improve its structural stability and surface area to volume ratio capacity, substantial efforts such as doping (Valero-Romero et al. 2019), hetero-junction with equivalent or/and different bandgap materials (Wang et al. 2008)**,** dye sensitization (Macák et al. 2005), noble and non-noble metal deposition (An et al. 2009), etc. have been applied. Among those different modification techniques, nowadays due to its relative simplicity researchers prefer to form a heterojunction between two/more different band-gap semiconductor materials.

Furthermore, not only increasing efficiency and reducing the above-mentioned drawbacks, the recovery of the engaged photocatalysts from the solution, specifically using magnetic materials, is the current issue. This indirectly reduces cost and secondary contamination. In view of this, owing to their outstanding magnetic properties, being environmentally kind, and found abundantly, a number of researchers have investigated iron oxides (which has a narrow band-gap of ~2.2 eV) as a recovering agent (Wang et al. 2014). Furthermore, forming a couple between TiO_2 and iron oxide (γ-Fe_2O_3, α-Fe_2O_3, and Fe_3O_4) (Porter et al. 2018), can enhance a large number of adsorptive sites that assists the adsorption of organic dyes and heavy metals.

As suggested by Zeyan Wang et al. (2014), depending on the conduction band (CB) & valence band (VB) potentials and bandgap energies, the electronic arrangement of the semiconductor heterojunctions are categorized into the straddling gap, staggered gap, and broken gap. Among these, the staggered band structure has a high probability towards electron-hole (e^--h^+) separation and improving the capacity of the photocatalytic reaction. This has occurred due to the creation of a depleted layer at the interface of the two, which produces an electric field and then the diffusion of the photogenerated e^--h^+ out of the depletion layer. This intern reduces the recombination process and enhances the photocatalytic activity (Mamba and Mishra 2016).

Liquid-solid translation synthesis methods of metal oxides nanomaterial are largely used in order to regulate the shape, size, structural features of the nanomaterials. During synthesis controlling various parameters including size, shape, morphology, etc. leads towards better photocatalytic efficiency (Li et al. 2016). Among a number of methods used to control these parameters during synthesis of metal oxides, the sol-gel (Wahyuningsih et al. 2018), impregnation (Abebe and Ananda Murthy 2018), hydrothermal (Sharma et al. 2018), co-precipitation (Shojaie et al. 2018), solvothermal (Jin et al. 2017), ultrasonic-microwave (Lin and Mehrvar 2018), etc. are the familiar ones. However, most of these methods involve the use of expensive equipment and chemicals. Among those methods, the co-precipitation, sol-gel, and impregnation are preferable by their relative simplicity and inexpensiveness (Habibi and Karimi 2014).

In addition to photocatalysis, the sol-gel (Durães et al. 2011), co-precipitation (Porter et al. 2018), micelle and inverse micelle (Gromova et al. 2018), hydrothermal method (Nguyen et al. 2018), mesoporous/nanoporous (Huang et al. 2018), sonochemical (Rostami et al. 2018) and impregnation (Abebe et al. 2017) are also practiced for adsorption of pollutants. Furthermore, the most common techniques used for heavy metal treatment include reduction and precipitation (Katsou et al. 2011), coagulation-flocculation (Tang et al. 2016), electrocoagulation (Ding et al. 2018), adsorption (Monárrez-Cordero et al. 2018), and membrane and ultra-membrane filtration. Among those different techniques adsorption is the most common and popular method for adsorption of non-biologically degradable toxic heavy metals (Rivera et al. 2016).

In this regard, Mirmasoomi et al. (2017) synthesized TiO_2/Fe_2O_3 nanopowder by the ultrasonic-assisted impregnation method, and they found that this material showed good adsorption as well as diazinon photodegradation capability. Dai et al. (2019) noticed the great e^--h^+ pair recombination inhibition, better light absorption capability, and acetaldehyde and o-xylene degradation efficiency of Fe_2O_3 impregnated TiO_2 nanomaterials. Furthermore, as summarized in table 5 both Sun et al. (2018) and Singh et al. (2019) have fabricated TiO_2/Fe_2O_3 nanocomposite by the same impregnation methods and found its better degradation activity. However, nowadays using globally harmless solvent during synthesis has countless bright side towards safety, simplifying the synthesis procedures, and reducing the cost. The current research work is also modifying the existing methods that use organic solvent by water only (Abbas et al. 2016), suggesting that this method yields a good quality of nanostructured materials with organic solvent-free and lower production cost. As suggested by Alder et al. (2016), the safety commonly related to solvents that have high vapor pressures and low boiling points and leading to explosions.

This work also concentrates on the synthesis of TIOs nanomaterials for photocatalytic degradation of methyl blue and using environmentally benign water as a solvent and impregnation method. Applying slight modification during synthesis (such as reducing the calcination temperature to 450 ^oC and decreasing the aging time), the adsorption capacity of the material was tested on the removal of lead ion from aqueous solution. The explanation of adsorption isotherms were tested by Langmuir, Freundlich, FG, D-RK, Temkin, and FH models. For adsorption-reaction kinetics study PFO, PSO and Elovich models and for adsorption-diffusion kinetic studies, the IPD model was used. The effect of temperature and desorption experiments were also conducted.

1.1. Objectives

1.1.1. General Objective

- To synthesize, characterize, and study the adsorption and photocatalysis activities of Ti-Fe binary nanocomposite oxides.

1.1.2. Specific Objectives

- To synthesize Ti-Fe binary nanocomposite oxides
- To characterize the physical properties of as-synthesized material using SEM-EDX, XRD, UV-Vis, FT-IR, BET, and TGA-DTA analytical techniques.

- To study the dye degradation and lead ion adsorption activities of the as-synthesized mixed oxides

1.2. Statement of the Problem

In modern economies, various types of activities (such as agriculture, industry, and transportation) produce a large number of waste and new types of toxic pollutants. Since several industries including paper, textile, cosmetics, plastics, printing, food processing, pharmaceutical leather, and dye manufacturing use dyes for their purpose, water pollution has become a common problem for many countries. It is reported that about 1-20% of the total world production of dyes is lost during the dyeing process and therefore a large quantity of these dyes appears in wastewater. Many of these dyes also cause health problems such as allergic dermatitis, skin irritation, cancer and mutation in humans (Jalil et al. 2010; Zuohua Wang et al. 2010). Among numerous pollutant sources, the textile industries are one of the highest water use and polluting industries in the world. Since, the main disposal areas for those wastes are the soil, air, and water; indirectly those organic and inorganic pollutants can pose a health risk. Due to the lack of water treatment, the contradiction between water pollution and worldwide industrial water requirement forces industrial manufacturers to adopt cleaner production technologies to save water (Rather et al. 2019).

1.3. Significance of the Study

Nowadays, the agricultural based economy is moving to the industrial based economy. Shifting this agricultural dependent economy to industrial based economy led to emission of massive pollutants. During this transformation when these industries were constricted and start their work, emission of their waste product as a solution to the rivers, lakes was is certainty. These waste products which are released from the factories will pollute our environment and also affect the health of the community as well as the health of animals which are present around those factories. The productivity of the farm lands were also decreases if the farmers use that waste water for irrigation purpose. Due this reason removing those toxic pollutants should be the first and the most important things.

Among different methods used to remove and dissociate those toxic organic pollutants from polluted water without secondary pollution, the nanotechnology dependent heterogamous adsorption and adsorption-photocatalysis techniques were suggested as a simple and efficient one. However, depending on different advantages even if bare metal oxides are superior for

adsorption-photocatalysis, several drawbacks including the electron-hole recombination, lack of visible light absorption, surface area enhancement, photo corrosion under UV irradiation, etc. are the major problems. Besides, unless the catalyst is regenerated/recycled from the solution it may become toxic, especially, if it's in the nanometer range. During the synthesis of the photocatalyst materials, up to now, many researchers use organic solvents. It is reported, in fact, that these organic solvents particularly that has high vapor pressures and low boiling points can cause dangerous explosions (Alder et al. 2016).

Even if TiO_2 has better strong oxidizing power, good stability, and environmentally compatible, the visible light absorption ability of it is poor (Qamar et al. 2015). To make it visible light active photocatalyst, forming a heterojunction with different bandgap materials is the ideal way. As much as possible, this work also struggles to make TiO_2 visible light active photocatalyst material by forming heterojunction with iron oxide materials. Therefore, by taking into consideration the indicated problems of pollutants and techniques, this work has been proposed to reveal regarding modification and improvements for each stated difficulty by forming the binary and ternary metal oxides for the adsorption and degradation of pollutants.

1.4. Expected output/deliverables

Successful completions of this research work play an invaluable role in the concept of adsorption and adsorption-photocatalysis pollutant remediation techniques as well as waste water treatment. The occurrence of dissolved inorganic ions is rather common in dye-containing industrial wastewater. Often, wastewater contains a mixture of pollutants, organic solvents as well as dissolved organic matter and humic substances, if mixed with other waste streams. These substances may compete for the active sites on the photocatalyst surface or deactivate it and, subsequently, decrease the degradation rate of the target dyes. Alternatively, they may act as light screens, thus reducing the photon receiving efficiency. Furthermore, anionic species present with the wastewater may acts as h^+ and $^{\bullet}OH$ scavengers and cationic species also decreases the reduction of O_2 by the conduction of electrons, subsequently blocks the formation of highly oxidizing agent and reactive oxygen species ($O^{2\bullet-}$/$^{\bullet}OOH$, $^{\bullet}OH$) (Konstantinou and Albanis 2004). However, if well-organized optimizations work were conducted on these negative effects, the synthesized materials become effective for real wastewater treatment.

2. Literature Review

2.1. Sources that Result in Water Pollution

In general, the sources that result in water pollution can be classified as point and nonpoint sources (Malik et al. 1993).The former one contains pollutants that are discharged from industries, septic materials, animal feedlots, mines and oil industries, and so forth into water sources (Yang et al. 2010). The latter one includes runoffs from agriculture, sediment, animal wastes, and so forth (Carpenter et al. 1998). According to the Environmental Protection Agency (EPA), nonpoint sources are claimed to be the major cause of aqueous pollutants.

According to the classification by the EPA, the most commonly observed hazardous wastes that threaten the global aquatic system can be divided into four groups: (i) hazardous wastes from nonspecific industrial processes, (ii) hazardous wastes from specific industrial sources, (iii) commercial chemical products, and (iv) toxic wastes. The EPA estimates that the above-mentioned pollutants have been increasingly detected during the past few decades in rivers, lakes, and oceans.

2.2. Removal Techniques

Continuous increase of pollutants in water bodies has necessitated the need to develop cost-effective methods for their removal. Destroying the pollutants to benign chemicals and/or removing these pollutants from contaminated water are imperative for a green environment. There are numerous treatment processes that have been applied for pollutant removal from wastewater, such as biodegradation (Papic 2004), coagulation (Stock et al. 2000), precipitation and adsorption (Jain et al. 2007), sonochemical degradation (Ning et al. 2007), micellar enhanced ultrafiltration, and Advanced oxidation process (AOP). Though these methods are considered as efficient methods for pollutant removal, each method has its own benefits and drawbacks. From these adsorption is an effective and well-known process and has been widely explored as an alternate technique compared with the other waste removal methods due to the lower cost, flexibility and simplicity of design, and ease of operation. Moreover, adsorption does not result in production of any harmful substances. But it does not degrade the pollutant since the adsorption process merely removes pollutants from the aqueous phase and transfers them onto a solid matrix (Braslavsky 2007). Thus, AOP have emerged as efficient methods for the mineralization of organic pollutants.

Semiconductor-mediated photo-catalysis is a well-established technique for pollutant degradation. Photo-catalysis can be defined as a "catalytic reaction involving the production of a catalyst by absorption of light" (Khin et al. 2012). The appropriate positioning of valence (VB) and conduction (CB) bands in semiconductors (Figure 1a) makes them suitable materials for the absorption of light and photocatalytic action. Nano-crystalline titanium dioxide (NTO) is a multifunctional semiconductor photocatalyst that can be an energy catalyst (in water splitting to produce hydrogen fuel), an environmental catalyst (in water and air purification), or an electron transport medium in dye-sensitized solar cells (Figure 1b) (Gaya and Abdullah 2008). Compared to other available semiconductor photocatalysts, NTO is unique in its chemical and biological inertness, photo-stability (i.e., not prone to photo-anodic corrosion), and low cost of production. Photocatalytic water and air purification using NTO is a predominant advanced oxidation process (AOP) because of its efficiency and eco-friendliness (Gaya and Abdullah 2008).

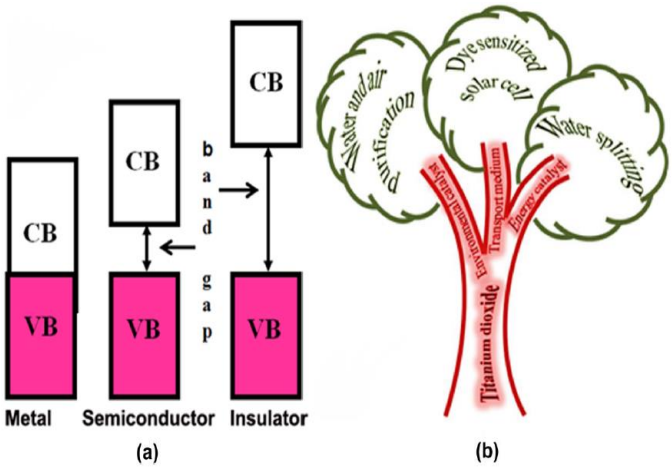

Figure 1. (a) VB and CB positions in metals, semiconductors, and insulators; (b) Tree diagram showing applications of TiO_2.

2.2.1. Advanced oxidation process

Advanced oxidation process (AOP) is an oxidation technique, which typically uses ambient conditions (room temperature and atmospheric pressure). Several AOP techniques such as ozonation, H_2O_2 photolysis, Fenton process, photo-Fenton process, and heterogeneous photo catalysis have been explored for the elimination of pollutants, particularly from water sources. These AOP techniques destroy the pollutants by chemical oxidation or reduction. In particular, AOP relies on the production of hydroxyl radicals ($^{\cdot}OH$) Figure 2, which are short-lived, extremely highly reactive species and attack most organic molecules with rate

constants of 10^{-6}– $10^{-9}M^{-1}s^{-1}$. Moreover, the versatility of AOP is enhanced by different possible ways for the production of hydroxyl radicals.

From these different methods of AOP, due to low-cost and environmentally benign treatment technology, extensive research interest has been devoted into heterogeneous photocatalysis and promising results have been obtained for the removal of highly toxic and non-biodegradable pollutants that are commonly found in industrial wastewaters. It is a process, which embraces a large variety of reactions such as oxidation, dehydrogenation, metal deposition, organic synthesis, water splitting, photo-reduction, hydrogen transfer, isotopic exchange, disinfection, anticancer therapy, water detoxification, and gaseous pollutant removal (Ibhadon and Fitzpatrick 2013). Heterogeneous photocatalysis is considered as an effective AOP technique, particularly for air and water purification treatment. Heterogeneous photocatalysis can be carried out in gas or liquid phases, and the overall process can be explained by five different reactions: (i) transfer of the reactants in the fluid phase to the surface, (ii) adsorption of at least one of the reactants, (iii) reaction in the adsorbed phase, (iv) desorption of the product(s), and (v) removal of the products from the interface region

Commonly, the heterogeneous photocatalysts are semiconductors, such as titanium dioxide (TiO_2), which can produce electron-hole pairs by the illumination with photons whose energy is equal to or greater than the bandgap of the semiconductor as shown by

$$TiO_2 \xrightarrow{hv} e^-_{CB} + h^+_{VB} \quad (1)$$

The electron-hole pairs then dissociate into free photoelectrons in the conduction band and holes in the valence band are produced (Bizarro 2010). The photo efficiency can be reduced by the surface or volume recombination of the electron-hole pairs either in the bulk or at the surface as depicted in Figure 2.Thus, recombination is undesirable and is detrimental to the photocatalytic activity.

In this photocatalysis process, the contaminant molecule gradually breaks down by its reaction with highly reactive oxidative species (ROS), such as $HO^{\cdot}$, $O_2^{\cdot -}$, and $HOO^{\cdot}$, which can be generated during the illumination process by the following equations (Bizarro 2010):

$$h^+_{VB} + OH^-_{ads} \rightarrow OH^{\cdot}_{ads}$$

$$h^{+}_{VB} + H_2O \rightarrow HO^{\cdot} + H^{+}$$

$$2HO^{\cdot} \rightarrow H_2O_2$$

$$2H^{+} + O_2 + 2e^{-} \rightarrow H_2O_2$$

$$2H_2O + h^{+}_{VB} \rightarrow H_2O_2 + 2H^{+}$$

$$H_2O_2 \xrightarrow{h\nu} 2HO^{\cdot}$$

$$e^{-}_{CB} + O_{2\,(ads)} \rightarrow O_2^{\cdot -}$$

$$O_2^{\cdot -} + 2H^{+} + e^{-}_{CB} \rightarrow H_2O_2$$

$$O_2^{\cdot -} + H_2O_2 \rightarrow HO^{\cdot} + HO^{-} + O_2$$

Among all these ROS, it has been widely noted that hydroxyl radicals are the most potent and important species responsible for the degradation of pollutants. Table 1 shows a comparison of the various removal techniques.

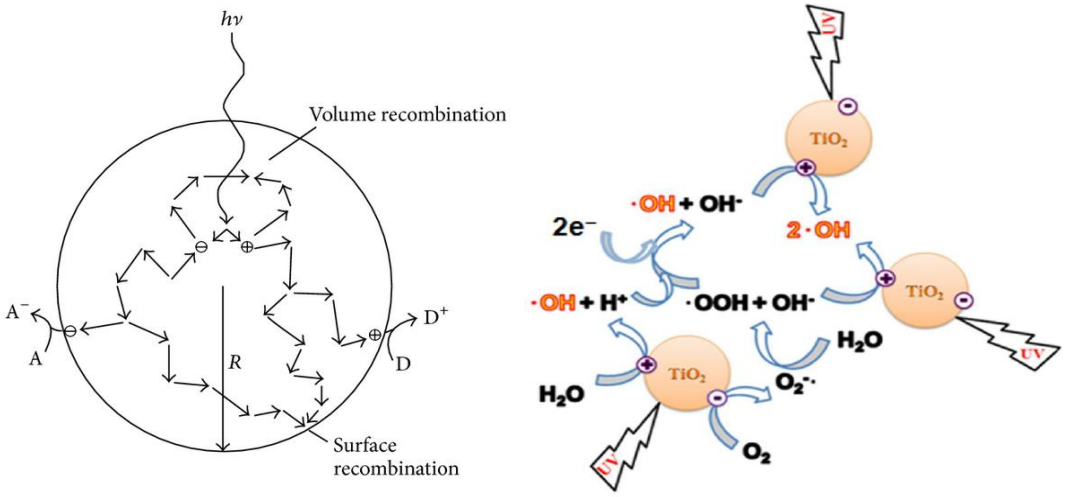

Figure 2. (a) Recombination of electrons and holes within a semiconductor particle in the presence of acceptor (A) and donor (D). (b) Photo-catalytic generation of hydroxyl radicals (Lazar et al. 2012).

Frank and Bard (1977) have reported the heterogeneous photo-catalytic oxidation of cyanide and sulfite in the presence of several semiconductors that include TiO_2, ZnO, CdS, Fe_2O_3, and WO_3, in aqueous medium under sunlight. It was noticed that, TiO_2, ZnO, and CdS showed good activity for cyanide oxidation, and no oxidation was seen using Fe_2O_3 and WO_3. In addition, the rates of the photo-catalytic oxidation were found to be greater for sulfite than cyanide. Among these oxides, titanium dioxide (TiO_2) is an effective semiconductor material that has been explored for numerous applications including

adsorption, heterogeneous photo-catalysis for splitting of water (Kho et al. 2010), solar cell applications (Chou et al. 2007), and degradation of pollutants.

Among numerous semiconductor materials, there has been considerable interest in the use of TiO_2 as a photocatalyst to degrade a variety of pollutants in water (Konstantinou and Albanis 2004). However, the photocatalytic performance of TiO_2 is significantly constrained by the fast recombination of the photo-generated electron-hole pair. In addition, its large bandgap energy (3.2 eV in anatase), low adsorption efficiency, surface area, and porosity restrict the widespread application of TiO_2 photo-catalysts. In order to reduce these drawbacks and to improve its structural stability and surface area to volume ratio capacity, substantial efforts such as doping (Valero-Romero et al. 2019), hetero-junction with equivalent or/and different bandgap materials (Wang et al. 2008)**,** dye sensitization (Macák et al. 2005), noble and non-noble metal deposition (An et al. 2009), etc. have been applied. Among those different modification techniques, nowadays due to its relative simplicity researchers prefer to form a heterojunction between two/more different band-gap semiconductor materials.

2.3. Types of Photocatalysts and their Characteristics

A number of solids can be referred to as photocatalysts and as mentioned earlier, metal oxide semiconductors are considered to be the most suitable photocatalysts due to their photocorrosion resistance and wide band gap energies. Table 2 provides the band gap energies at corresponding wavelength for well-known semiconductors. TiO_2 stands out as the most effective photocatalyst and has been extensively used in water and wastewater treatment studies, because it is: cost effective, thermally stable, non-toxic, chemically and biologically inert and is capable of promoting oxidation of organic compounds (Mandelbaum et al. 1999). The photo-catalytic activity of TiO_2 is dependent on surface and structural properties which include crystal composition, surface area, particle size distribution, porosity and band gap energy (Ahmed et al. 2011).

Table 1. Different removal techniques and its advantage(s) and disadvantage(s).

Removal techniques	Advantage(s)	Disadvantage(s)
• Electrochemical oxidation	Does not require auxiliary chemicals, high pressures, or high temperatures.	Low selectivity and low reaction rates.
• Biological process	Ecologically favorable process.	High capital and operational cost. Handling and disposing the secondary sludge pose problems.
• Adsorption	Cost-effective method. Easy availability and operation. Most profitable process and more efficient than the conventional methods (i.e., precipitation, solvent extraction, membrane filtration, etc.).	Merely removes the pollutants from one phase (aqueous) to another (solid matrix). Expensive process for regeneration especially if the pollutants are strongly bound to the adsorbents.
AOP		
(i) Ozonation	Powerful oxidation technique oxidizes a large number of organic and inorganic materials.	More complex technology and requires high Capital/operational cost. High electric consumption.
(ii) UV	An effective method that typically does not leave any byproducts which are harmful to the environment.	Less effective if the wastewater has high amounts of particulates which can absorb UV light.
(iii) UV/H_2O_2	An effective technique in the oxidation and mineralization of most organic pollutants. Ease of formation of ·OH radicals.	Less effective, when the wastewater has high absorbance. High operational cost.
(iv) $O_3/UV/H_2O_2$	Most effective process due to the fast generation of ·OH radicals. Can treat a wide variety of contaminants.	Needs to compete with high turbidity, solid particles, and heavy metal ions in the aqueous stream. High operational cost.
(v) Fenton reaction	Simple process. Easy availability of chemicals.	Production of sludge iron waste and handling the waste pose logistical problems.
(vi) Photo-Fenton reaction	Reduction of sludge iron waste compared to original Fenton reaction. Effective and fast degradation. Long-term stability at high temperature.	Needs a controlled pH medium for better performance. Could form byproducts that can be harmful to the environment.
(vii) Heterogeneous photocatalysis	Resistance to attrition. Low-cost and environmentally kind treatment technology.	Requires efficient catalysts that can absorb in the visible region.

TiO_2 is also known as titania, titanic oxide, titanium white, titanic anhydride, or titanic acid anhydride. It is prepared using ilmenite and rutile in crystalline forms called anatase and rutile. The anatase form is achieved by processing of titanium sulphate, which is achieved when ilmenite is treated with sulphuric acid. Rutile crystalline form is obtained when raw rutile is chlorinated and the resulting titanium tetrachloride is subjected to vapor phase oxidation. When photon energy (hv) of higher than or equal to the band gap energy of TiO_2 is illuminated onto its surface, typically 3.2 eV (anatase) or 3.0 eV (rutile), the lone electron is photo-excited to the empty conduction band in femto-seconds. Degussa P_{25} which is the most widely used form of TiO_2 is composed of 75% anatase and 25% rutile and has a specific BET surface area of 50 m^2/g. The high effectiveness of D_{25} is related to the inhibition of recombination process on TiO_2 (e_{CB}^-/h_{VB}^+) due to the smaller band gap of rutile that absorbs photons and generates electron-hole pairs and the electron transfer from the rutile conductive band to the electron traps occurs in the anatase phase (Hurum et al. 2003).

Table 2.Band gap energies of various semiconductors at relevant wavelengths.

Semiconductor	Band gap energy (eV)	Semiconductor	Band gap energy (eV)
Diamond	5.4	WO_3	2.76
Cu_2O	2.172	Si	1.170
ZnS	3.60	Fe_2O_3	2.3
TiO_2	3.030	PbS	0.286
SnO_2	3.54	PbSe	0.165
ZnO	3.36	ZrO_2	3.87
CdSe	1.7	Ge	0.744

2.5. Factors Affecting the Degradation Performance

2.5.1. Catalyst loading

The amount of photocatalyst being directly proportional to the overall photocatalytic reaction rate, the concentration of the TiO_2 particles affects the overall photocatalysis reaction rate in a true heterogeneous catalytic regime. However, when the amount of TiO_2 is above certain level (saturation stage), the light photon adsorption co-efficient decreases radially and the excess photocatalyst can create a light screening effect that leads to the reduction in the surface area exposed to irradiation and thus reduces the photocatalytic efficiency of the process. A number of studies have reported the effect of TiO_2 loadings on the treatment efficiency of the photocatalytic reactor (Chong, Jin, et al. 2009). Although a direct comparison between these studies is difficult to be made due to the differences in the working geometry, radiation fluxes and wavelengths used, it was evident that the optimum dosages of photocatalyst loading were dependent on the dimension of the reactor.

2.5.2. pH of the solution

The effect of pH on the photocatalytic reaction has been extensively studied. Due to the fact that photo-catalytic water treatment is highly dependent on the pH as it affects the charge on the catalyst particles, size of aggregates and the position of conductance and valance bands. Furthermore the surface of the TiO_2 can be protonated or de-protonated under acidic or alkaline conditions, respectively according to the reaction given below.

$$TiOH + H^+ \rightarrow TiOH_2^+ \quad (6)$$

$$TiOH + OH^- \rightarrow TiO^- + H_2O \quad (7)$$

The point of zero discharge for P25 Degussa, commonly used form of TiO_2 is 6.9 (Kosmulski 2009). Therefore the surface of the TiO_2 is positively charged under acidic conditions and negatively

2.5.3. Reaction temperature

An increase in reaction temperature generally results in increased photocatalytic activity however reaction temperature >80^{o}C promotes the recombination of charge carriers and disfavor the adsorption of organic compounds on the titania surface. A reaction temperature below 80^{o}C favours the adsorption whereas further reduction of reaction temperature to 0^{o}C results in an increase in the apparent activation energy. Therefore temperature range between 20-80^{o}C has been regard as the desired temperature for effective photomineralization of organic content (Arslan-Alaton 2003).

2.5.4. Concentration and nature of pollutants

The rate of photocatalytic degradation of certain pollutant depends on its nature, concentration and other existing compounds in water matrix. A number of studies have reported the dependency of the TiO_2 reaction rate on the concentration of contaminants in water. High concentration of pollutants in water saturates the TiO_2 surface and hence reduces the photonic efficiency and deactivation of the photocatalyst. In addition to the concentration of pollutants, the chemical structure of the target compound also influences the degradation performance of the photocatalytic reactor. For example, 4-chlorophenol requires prolonged irradiation time due to its transformation to intermediates compared with oxalic acid that transforms directly to carbon dioxide and water, i.e., complete mineralization. Furthermore if the nature of the target water contaminants is such that they adhere effectively to the

photocatalyst surface the process would be more effective in removing such compounds from the solution. Therefore the photocatalytic degradation of aromatics is highly dependent on the substituent group. The organic substrates with electron withdrawing nature (benzoic acid, nitrobenzene) strongly adhere to the photocatalyst and therefore are more susceptible to direct oxidation compared with the electron donating groups (Chong, Lei, et al. 2009).

2.6. Wastewater and Water Quality Issues

Wastewater contains a number of pollutants and contaminants, including: (i) plant nutrients (nitrogen, phosphorus, potassium); (ii) pathogenic microorganisms (viruses, bacteria, protozoa and helminthes); (ii) heavy metals (e.g. cadmium, chromium, copper, mercury, nickel, lead and zinc); (iii) organic pollutants (e.g. polychlorinated biphenyls, poly-aromatic hydrocarbons, pesticides); and biodegradable organics (BOD, COD); and (iv) Micro-pollutants (e.g. medicines, cosmetics, cleaning agents).

All of these can cause health and environmental problems and can have economic/financial impacts (e.g. increased treatment costs to make water usable for certain purposes) when improperly or untreated wastewater is released into the environment; nutrient contamination and microbial water quality issues are considered further below.

2.4. Adsorption

Adsorption is a surface phenomenon in which adsorbate molecules bind to the adsorbent either through physical forces or chemical interactions or both. The three common mechanisms involved in adsorption include film diffusion, pore diffusion and surface reaction as shown in Figure 3 (Zhang et al. 2018). During those adsorbent-adsorbate contact processes, two main types of interaction namely, the physical (physisorption) and chemical (chemisorption) interaction are possible. As a guideline, the heat of adsorption with a magnitude between 5 and 40 kJ/mol indicates physisorption as the dominant adsorption mode, and between 40 and 125 kJ/mol indicates chemisorption (Zhou et al. 2014).

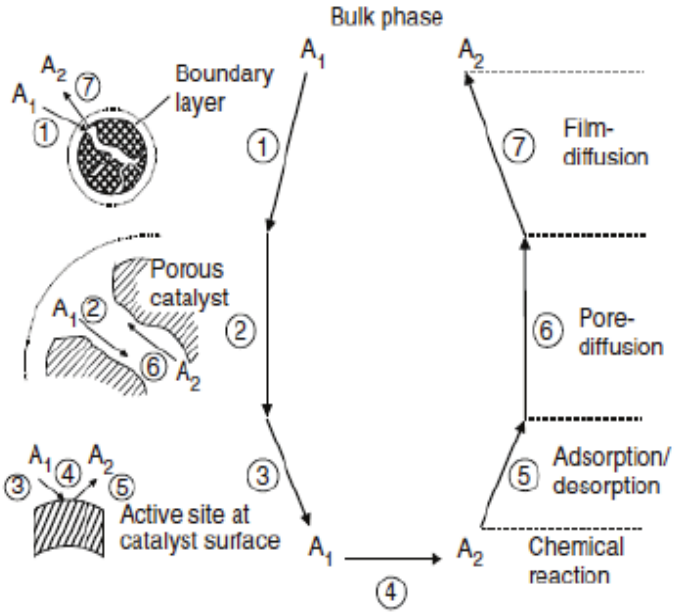

Figure 3. Individual steps of a simple, heterogeneous catalytic fluid-solid reaction $A_1 \rightarrow A_2$ carried out on a porous catalyst (Lin and Wang 2008).

Adsorption equilibrium statistics is the most important piece of information needed for a proper understanding of an adsorption process. A proper understanding and interpretation of adsorption isotherms are critical for the overall improvement of adsorption mechanism pathways and the effective design of the adsorption system. During adsorption isotherm study to understand the mechanism of adsorption, it is advisable to apply at least Langmuir, Freundlich, Dubinin-Radushkevich (D-RK), Temkin and Flory-Huggins (FH) adsorption isotherm model (equation 7-12). In addition, to interpret the time-dependent experimental data and to say the reaction is under control of adsorption-reaction or adsorption-diffusion, testing the pseudo first (PFO), pseudo second (PSO) and Elovich for adsorption-reaction and intraparticle diffusion (IPD) for diffusion-adsorption (equations 13-16) should be taken into consideration.

3. Materials and Methods for Adsorption-photocatalysis Study

3.1. Characterization Techniques and Reagents used

The physical properties of synthesized materials were characterized by scanning electron microscopy with energy-dispersive X-ray spectroscopy (SEM-EDX), X-ray diffraction (XRD), Fourier transform-infrared spectroscopy (FT-IR), thermogravimetric analysis-differential thermal analysis (TGA-DTA), Brunauer–Emmett–Teller (BET), UV-Vis spectrophotometer (SM-1600), and flame atomic absorption spectrophotometer (Model210/211 VGP) analytical techniques. SEM-EDX (ZEISS EVO 18), XRD (BRUKER D8 Advanced XRD), and BET analysis were conducted in India. The FT-IR (BRUKER IFS120 M Perkin Elmer) analysis was conducted in Addis Ababa University. And the TGA-DTA (DTG-60H) and additional XRD characterization test were done in Adama Science and Technology University. The other instruments used for this work are pH meter (MP 220), rotary shaker (Orbital shaker SO1 made in UK), magnetic stirrer, orbital shaker, hot air oven (Contherm 260 M), and Furnace. The optimizations of lead ion removal were conducted in Adama Science and Technology University. The dye degradation, adsorption isotherm, adsorption kinetics, thermodynamics, desorption test, were conducted in Haramaya University. The common reagents used are commercial TiO_2 powder, iron nitrate nine hydrated ($Fe(NO_3)_3.9H_2O$) (99.95 %, BDH chemicals Ltd, England), methyl orange dye (MO), NaOH, and NH_3.

3.2. Synthesis

All reagents used for the synthesis of TIOs nanomaterials were analytical grades. To load Fe_2O_3 on TiO_2, the impregnation method was used as reported by earlier researchers (Abebe and Ananda Murthy 2018; Mirmasoomi et al. 2017), with small modification such as replacement of water in place of organic solvent and using simple magnetic stirrer in place of ultra-sonication. In general, 0.1 M of TIOs materials were synthesized by adding TiO_2 powder in the aqueous solution of Fe $(NO_3)_3 \cdot 9H_2O$ with continuous stirring at 80 ^oC for 30 minutes. At this period, the homogenous woody color of the solution was observed. Later drop wise addition of NH_3 results in shifting of the pH of the solution to the basic range and giving the same color, but heterogeneous types of solution. Then, the aging (for two days), washing, drying (at 105 ^oC for16 h), and grinding procedures were accomplished. Finally, the obtained product was calcined at 500 ^oC. For the synthesis of single Fe_2O_3 and different composite; the same procedure were followed. The synthesized materials with different

percentage of Fe_2O_3 were designated as TIO-4, TIO-8, and TIO-12 for 4, 8, and 12 % of Fe_2O_3, respectively.

3.3. Adsorption-photocatalysis Study

The adsorption isotherm experiment in the dark was conducted by contacting 25 mL of different concentration of methyl orange (MO) in the range of 0.00001 - 0.01 mol/L with optimized 0.125 g of catalyst in 50 mL of Erlenmeyer flasks. The kinetics study in the dark was also done by taking various contact time in the range of 0 - 70 minutes. Furthermore, the photocatalytic reaction experiment was conducted by contacting 0.125 g of a catalyst with photocatalytically optimized 0.001 mol/L MO solution. Throughout the photocatalytic reaction, 10 mL of MO solution was taken at defined intervals, centrifuged to remove the catalyst and the residual concentration was measured using a UV-Vis spectrophotometer (Abebe et al. 2017).

4. Material and Methods for Adsorption of lead ion

4.1. Synthesis

Impregnation method was used to synthesize nano-sized TIOs binary oxides (Abebe et al. 2017). To prepare a 0.1M solution, initially iron (III) nitrate nonahydrate [(Fe $(NO_3)_3.9H_2O$] (99.95%) precursor salt were dissolved in deionized water and on this solution the powder TiO_2 was added. The temperature of the solution was adjusted to 80^oC on the hotplate with a constant stirring magnetic stirrer. Dilute NaOH was added drop-wise to increase the pH of the solution from 3 to 8 and aged with stirring continuously for one hour. The precipitate was centrifuged and washed repeatedly with alcohol and water. Finally, it was calcined for 2 hours at 450 ^oC after drying it in an oven at 110^oC overnight. The temperature reduced from 500 (that is used in adsorption-photocatalysis part) to 450 ^oC is to make more active to some extent by decreasing the crystallinity of the material. All chemicals/reagents used for this study have analytical grade purity.

4.2. Batch Adsorption Experiment

The adsorption experiment was carried out in 50 mL Erlenmeyer flasks having Ti-Fe oxide to lead ion aqueous solution ratio of 1:300 [0.1 g of Ti-Fe oxides: 30 mL of 35 mg/L of Pb $(NO_3)_3$]. Equilibration of the experiments was done on a rotary shaker. Then the obtained solution was filtered to separate the residue from the solution. The amount of lead ion deposited on adsorbent was obtained with the help of atomic absorption spectroscopy (AAS).

During the sorption experiments the pH of the solution, dosage, speed of agitation, time of contact and initial lead ion concentration were optimized.

To optimize the effect of pH on lead ion sorption, 0.1 g of the sorbent was taken into 50 mL of Erlenmeyer flask containing 30 mL of 40 mg/L lead ions, and varying the pH of the solutions as 2, 4, 6, 8, 10 and 12. To optimize the amounts of loaded powder; 0.05, 0.10, 0.15, 0.20, 0.25, 0.30 and 0.35 g of sorbent were taken. The effect of speed of agitation was optimized by adjusting the speed of the shaker as 40, 70, 100, 130, 160 and 190 rpm. During optimization, the first optimized parameters are kept at the optimized value and which is not optimized kept at a constant value. Sorption isotherms experiment was done by taking all the optimized values of parameters and varying lead ion concentration as 15, 25, 35, 45, 55, 65 and 75 mg/L in separate 50 mL Erlenmeyer flask.

The kinetics study was conducted by taking various contact time (10, 40, 70, 100, 130 and 160 min) and all the optimized values of parameters were used. In order to determine the effect of temperature on sorption phenomenon, all predetermined and optimized values of parameters were used and the temperature was established at 25, 35, 45 and 55^{o}C. Reproducibility study was done using lead ions loaded powder obtained after the sorption experiment and using optimized values and different pH solution (pH 2, 4, 6, 8, 10, 12). 0.1g of lead ion loaded binary oxide powder was added into six 50 mL of Erlenmeyer flasks having approximately 30 mL of distilled water and the pH of the solution was adjusted to 2, 4, 6, 8, 10 and 12 using acid and base.

5. Results and Discussion for Adsorption-photocatalysis

5.1. Characterization

5.1.1. XRD pattern

Matching the XRD spectra of TiO_2, α-Fe_2O_3, and the optimized composite (TIO-4) (Figure 4a), the 2θ and the respective Miller indices that appeared around 25^o(101), 37^o(004), 48^o(200), 53^o(105), 57^o(211), 60^o(213), 62^o(204), 68^o(116), 70^o(220), 74^o(215), 82^o(224) are assigned to the anatase TiO_2 (JCPDS Card No. 00-001-0562) and the other three peaks appeared at 32^o(104), 35^o(110), 40^o(113) (JCPDS Card No. 00-001-1053) are exactly assigned to α-Fe_2O_3 (Figure 4b), the same result was observed on previous works (Han et al. 2015; Li et al. 2015). The calculated average particle size D using Scherrer's equation is approximately equal to 59 nm,

$$D = \frac{K\lambda}{\beta\cos\theta} \quad (1)$$

Where K is constant and λ is the wavelength of the x-ray radiation. This result also has a close relationship with an approximate average size value obtained from the SEM image.
This calcination helps to, and increases the crystallinity to some degree.

Most of the times, to remove volatile impurities, to convert other forms of iron oxidize completely to α-Fe_2O_3 phase, to increase the crystallinity, and stability of the photocatalyst, increasing the calcination temperature become the significant factor. However, it is known that increasing the calcination temperature assists the growth of the crystalline particles. Therefore, optimizing the temperature becomes a matter of great concern. As shown on the TGA-DTA analysis, the material is almost stable above 380^oC. It is reported, in fact, the phase formation and crystallization of α-Fe_2O_3 is in the range of ~350 to 500 ^{o}C (Cuong et al. 2015). That is why the calcination temperature of the material was increased to the 450 and 500 ^{o}C than the optimized values on TGA-DTA (~400 ^{o}C) analysis. The obtained structure/geometry of TiO_2 and Fe_2O_3 with the help of mercury 3D structure visualization, exploration and statistical analysis of CSD search data software shows tetragonal (anatase) (ICSD-172916) and rhombohedral (ICSD-245851), respectively (Figure 4c).

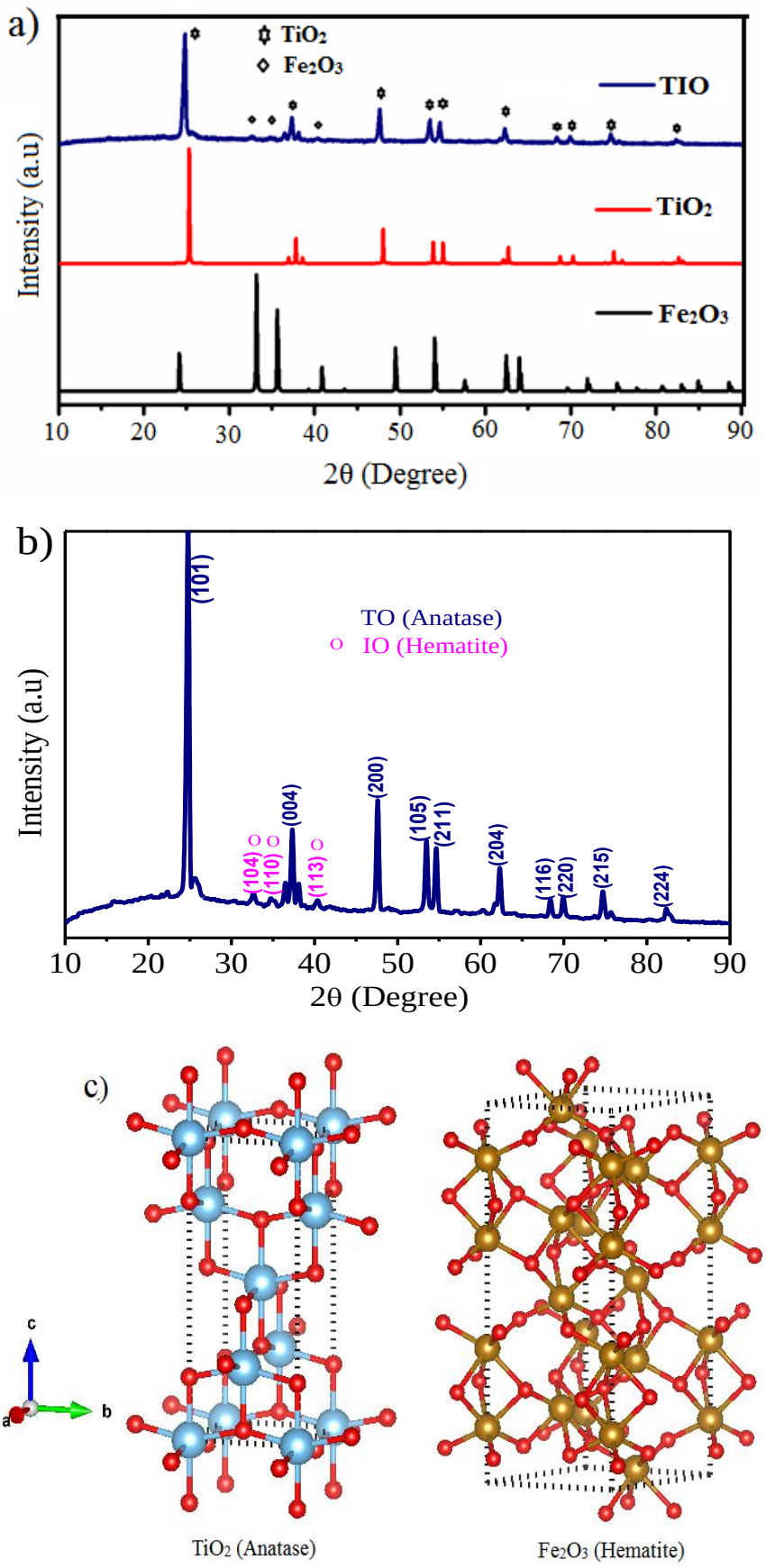

Figure 4. (a) XRD patterns of TiO_2, Fe_2O_3, and TIO-4; (b) XRD spectra of TIO-4 calcined at 500 ^oC; (c) Structure of TiO_2 and Fe_2O_3.

5.1.2. Optical properties

The investigated optical properties of TiO_2, α-Fe_2O_3, and TIOs using UV-Vis spectroscopic techniques are shown in Figure 5. As shown from the spectra, TiO_2 absorb only at around 400 nm due to its inherent direct transitions that has bandgap energy values of 3.2 eV (Figure 5a and b). However, TIOs exhibit two absorption bands at around 486 nm, due to direct band gap transitions, and 712 nm, which is attributed to indirect bandgap transitions (Saha et al. 2015). This shows that, the significant improvement of visible light absorption. As suggested by (Kılıç et al. 2015), owing to the unique half-filled electronic configuration of iron, by contracting the conduction band, it has the ability to form new intermediate energy levels inside the bandgap of TO. The created additional state leads to effective red-shift (longer wavelength) of the absorption threshold.

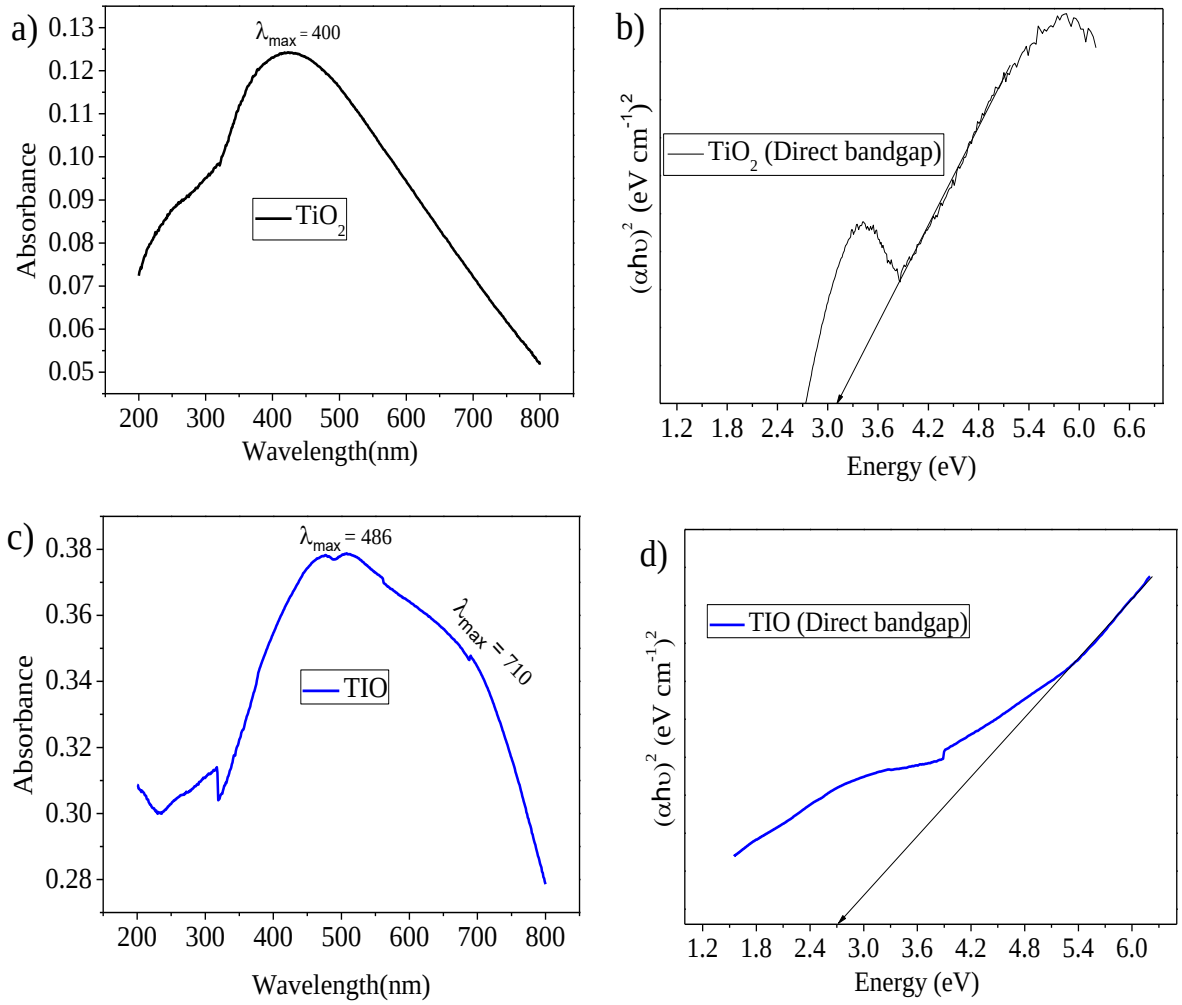

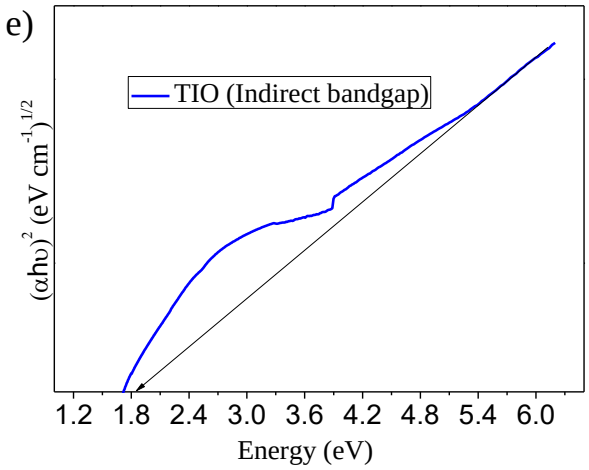

Figure 5. (a) and (b) UV-Vis spectra of TiO_2 and its Tauc plots; (c), (d), and (e) UV-Vis spectra of TIO-4 and its Tauc plots.

According to the photoelectric effect, the approximate energy bandgap (E_g) of the catalyst is equal to or less than the energy of the radiation (hν),

$$E_g = \hbar\left(\frac{c}{\lambda_{max}}\right) \quad (2)$$

Where c, $\hbar$, and λ_{max} are the speed of light, planks constant, and maximum wavelength, respectively. From this theoretical relation, the calculated approximate bandgap energy for TIO at 486 nm (Figure 5c) is equal to 2.55 eV. This value also has a close relation with the value obtained from direct bandgap Tauc plots value (Figure 5d) and the obtained bandgap value using indirect Tauc plots is 1.9 (Figure 5e).

5.1.4. The surface area and pore distribution study

For the synthesized nanocomposite material to be efficient photocatalyst, the optimal porosity and high surface area (low particle size) are the two crucial factors. From Brunauer–Emmett–Teller (BET) study, N_2 adsorption-desorption measurement carried out at 77 K (Figure 6a), the synthesized TIOs material was found to exhibit type IV isotherm with a sharp increase of the adsorbed volume starting from P/P_0= 0.97. This confirms the presence of well-developed mesoporous TIO nanostructured materials. The shifting of the hysteresis loop to the higher as the relative pressure (p/p_o) approaching to 1 indicates the presence of macroporous particles with size greater than 50 nm, this assists the approximate XRD particle size interpretation (59 nm). Furthermore, it is also confirmed by the presence of mesopore peaks around ~ 21, 44,

79, and 124 nm on the pore size distribution curve (Figure 6b) (Liu et al. 2016). The obtained BET surface area and pore volume value were found to be 71.56 m^2/g and 0.076 cm^3/g, respectively. Due to high surface area behavior of α-Fe_2O_3, the impregnation of it enhances the specific surface area of TIOs, so improving the adsorption capacity and photocatalytic efficiency (Subramonian et al. 2017a). From the equivalent, Barrett–Joyner–Halenda (BJH) pore-size, the obtained mean pore diameter for TIO was found to be 2.43 nm.

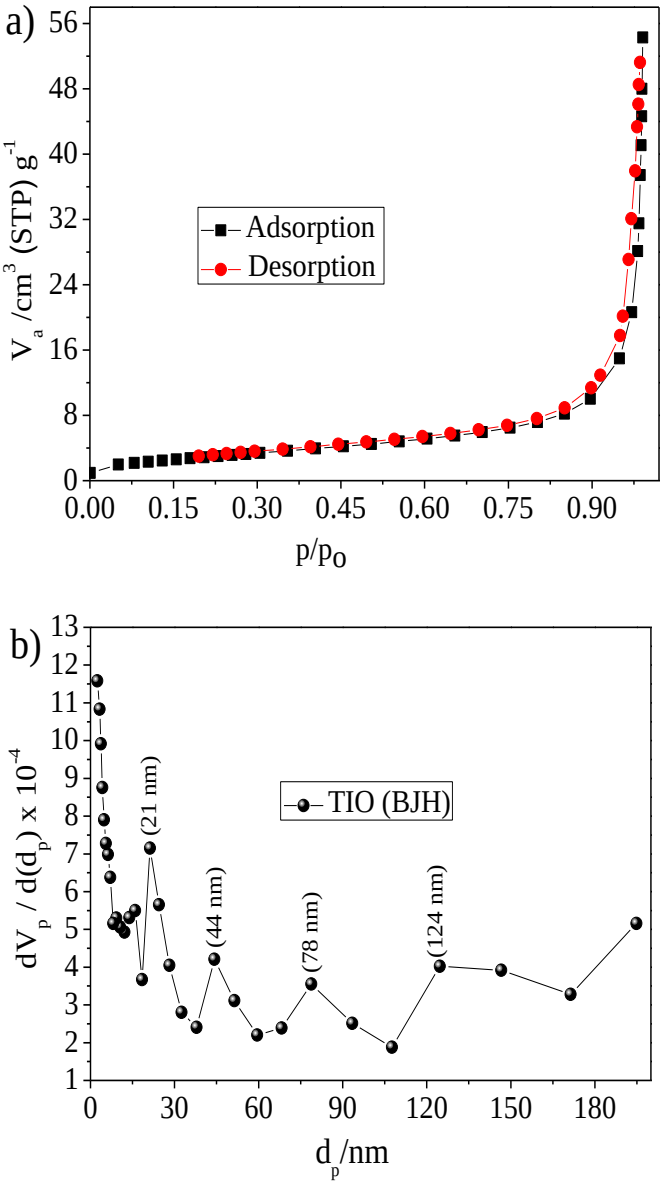

Figure 6. (a) Barrett–Joyner–Halenda N_2 adsorption isotherm (b) BJH spectra of TIO-4 calcined at 500 ^oC.

5.1.5. Morphology study

The morphology of TIO surface obtained from the SEM image (Figure 7) depicts the presence of irregular size and shapes of the particles. In between these particles, a porous space was observed which is believed to be advantageous to enhance the adsorption of MO dye during the adsorption-desorption period.

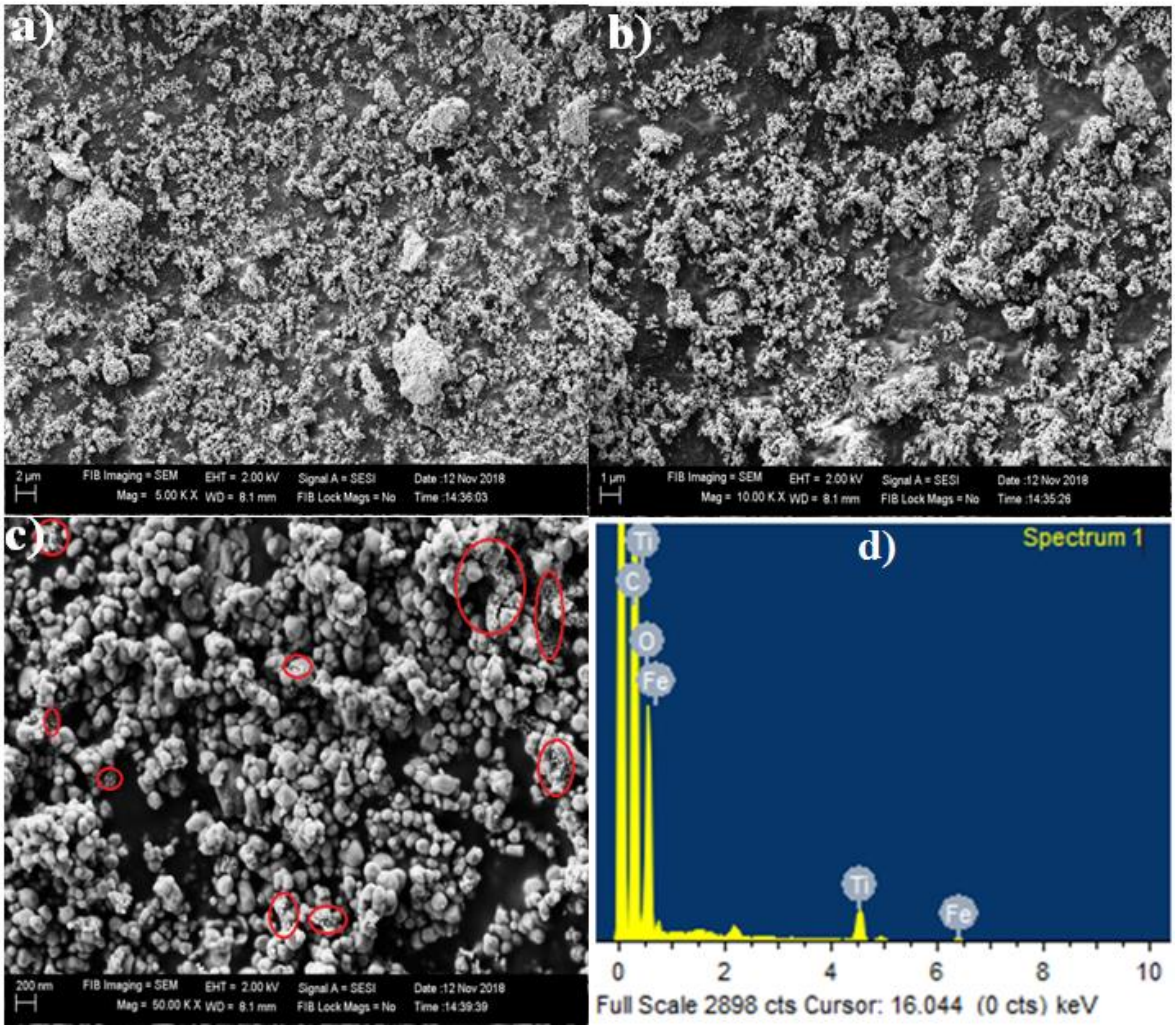

Figure 7. SEM-images with different magnifications (a, b, and c) and (d) EDX spectra of TIO-4 calcined at 500 ^{o}C.

The smaller sized particles dispersed throughout the matrix of TiO_2 and present as impurities (assigned as a spherical red mark in Figure 7c) are most probably for impregnated α-Fe_2O_3, a similar result was also reported on previous work (Jamalluddin and Abdullah 2011). Furthermore, as explained by Kılıç et al. (2015), as the surface roughness increases with increasing of the grain size, it is beneficial to solar conversion efficiency through enhancing the contact surface area among photoanode films, dye molecules, and organic pollutants.

Therefore, increasing the particle size to some extent has positive effect on photocatalytic reaction. The EDX analysis (Figure 5d) also confirms the presence of all the expected elements of Ti, Fe, and O. The appearance of C on the spectra may be from the standard used during analysis.

5.2. Adsorption-photocatalysis Study

5.2.1. Optimization

During adsorption studies in the dark, the optimum concentration is found to be 0.0005 mol/L (Figure 8). Furthermore, during the photocatalytic reaction optimization of both catalyst mass m and initial concentration of MO, up to the formation of the plateau, the reaction rate r (k_{app}) has a linear relationship to the mass of the catalyst and concentration of the MO. The optimum dose and MO concentration is found to be 0.125 g and 1 x 10^{-3} mol/L, respectively (Figure 9 & 10).

This linear increment is due to the availability of free active sites n_t on the surface of the catalyst, which is calculated by,

$$n_t = m \times S_{EBT} \times d_s, \quad (3)$$

Where, S_{BET} is the specific surface area of the catalyst and d_S is the areal density of the sites. As suggested by Boehm (1966), the maximum areal density value is estimated to be $\leq 5\times10^{18}$ m^2/g.

Calculating the approximate minimum number of MO that ought to be converted by 0.125g of bare TiO_2 with S_{BET} value of 50 m^2/g becomes 31.25×10^{18} molecules/g or 5.19×10^{-5} mol. The rough estimated minimum amount of molecules or moles that was converted by TIOs whose S_{BET} value of 71.56 m^2/g and 0.125 g of catalyst become 44.72 x 10^{18} molecules/g or 7.43 x 10^{-5} mol. Determining the ratio of MO degraded by TIOs (1 x 10^{-3} mol) to minimum requirement (7.43 x 10^{-5} mol), i.e. the n/n_{min} value becomes 13.46. Therefore, it's possible to say that, about 13.46 times more than the expected minimum amount was degraded.

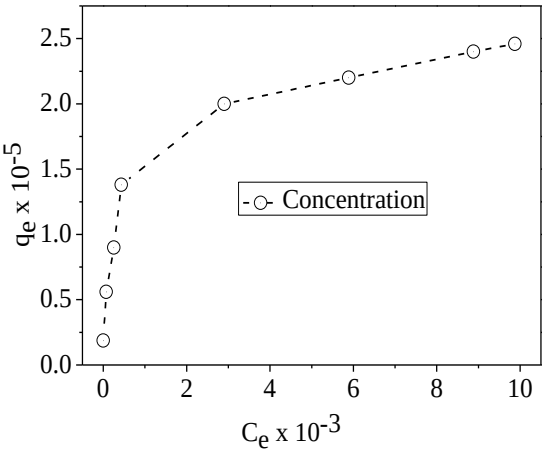

Figure 8. Concentration optimization during adsorption-desorption equilibration time in dark.

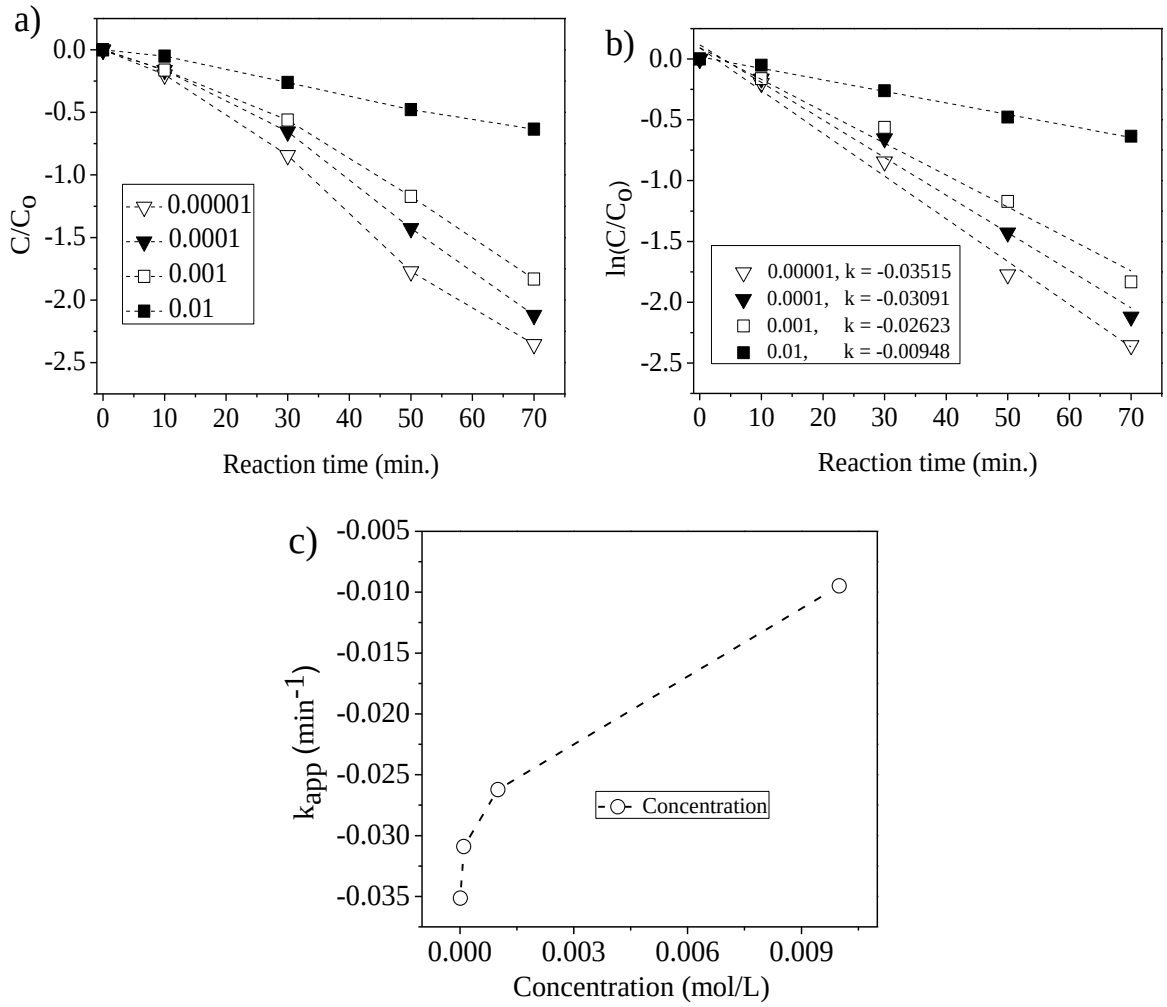

Figure 9. Concentration optimization during irradiation; (a) and (b) the pseudo first order kinetics plots of MO decolourisation, (c) the apparent rate constant verses concentration plots of pseudo first order kinetics.

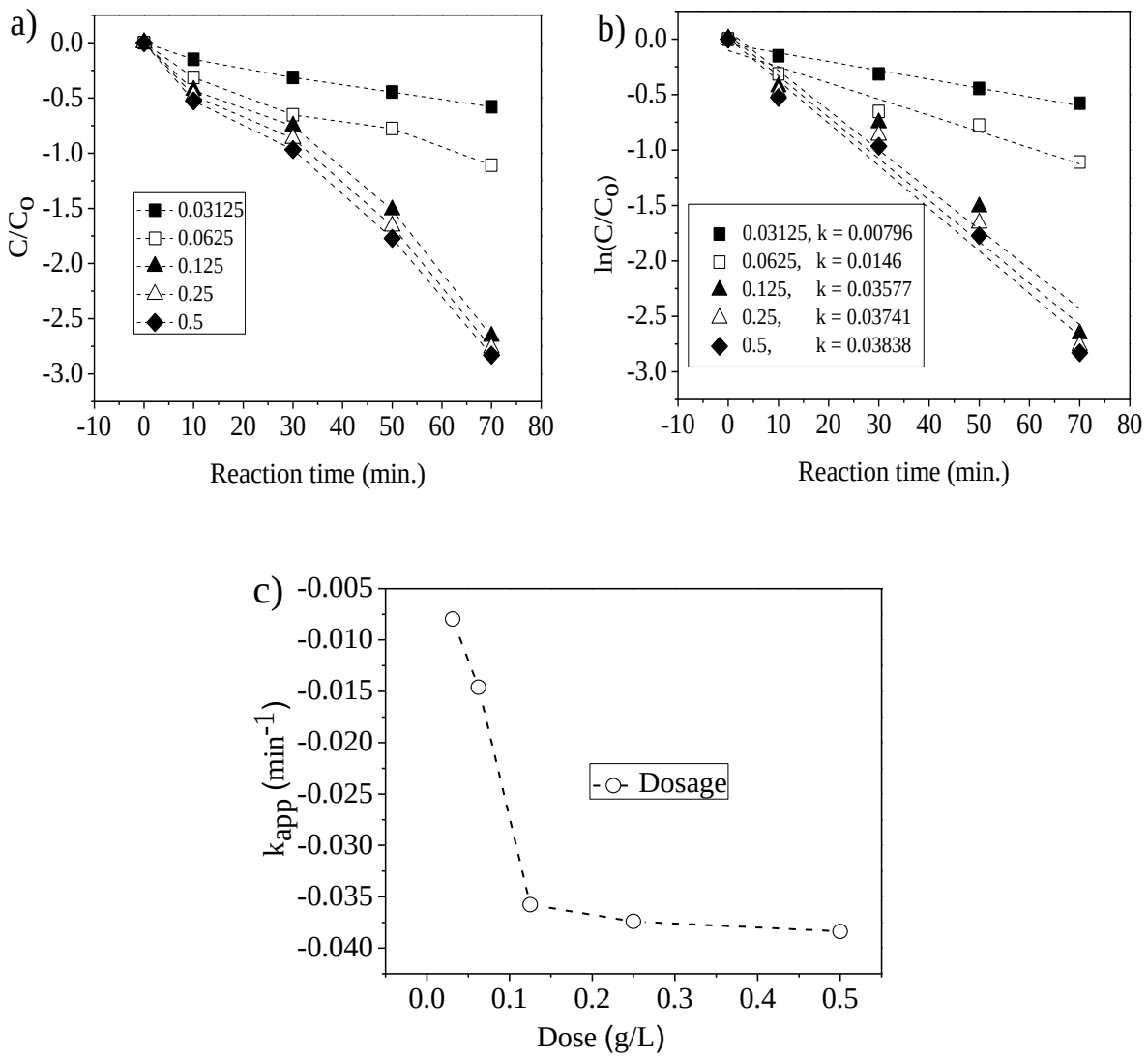

Figure 10. Dose optimization during irradiation; (a) and (b) the pseudo first order kinetics plots of MO decolourisation, (c) the apparent rate constant verses dosage plots of pseudo first order kinetics.

It's known that in aqueous solution, due to the presence of $-SO_3^-$ functional group on MO, it develops negative charge. As suggested by Bendjabeur et al. (2017), at more acidic pH the surface ionized to the more positively charged ($TiOH_2^+$) and creates attractive interaction between MO and the TIOs photocatalyst, this suppresses the degradation efficiency. In converse changing the pH of the solution to alkaline, due to reaction with OH^- the surface of the catalyst becomes negatively charged (TiO^-) and create a repulsion interaction. The obtained optimum pH value for this study is 4.

Furthermore, as indicated by Ohtani (2010), due to large photo adsorption coefficient values of MO dye, it may not be possible to show a turnover of the photocatalyst, therefore standardization using dye may not work. Furthermore, due to the complete chemical reaction nature of the photocatalytic reaction, it should be measured in terms of absolute physical amount in units of mole. Therefore, for the entire subsequent experiment on this work, the measurement was done in the units of mole.

5.2.2. Adsorption Isotherms

Adsorption equilibrium statistics is the most important piece of information needed for a proper understanding of an adsorption process. From the mass balance the equation becomes:

$$m\,(q-q_e) = (C_0 - C_e)v \qquad (4)$$

To determine the equilibrium relationship at $q_o = 0$, the relation becomes:

$$q_e = \frac{v}{m} x\,(C_o - C_e) \qquad (5)$$

The percent of sorption (%) were calculated using equation:

$$\% = \frac{C_o - C_e}{C_o} * 100 \qquad (6)$$

Where: C_o = the initial concentrations (mg/L) and C_e = equilibrium concentrations (mg/L) of lead ion, q_e = adsorption capacity of adsorbent (mg/g), V = the volume of reaction mixture (L), m = the mass of adsorbent used (g).

Ideally the first-order kinetics works in homogenous solution. Therefore, in photocatalysis, to study the rate of reaction using first-order reaction kinetics, the reaction should be under control of the diffusion process, i.e. the rate-determining step (the slowest step) should be adsorption of pollutant on the surface of the catalyst. On the contrary, if its surface reaction is limited i.e. the lowest step is the reaction of e^- and h^+ with surface adsorbed MO pollutant, unless it follows Henry/Langmuir-type of equations, the photocatalytic reaction rate may not obey the first order rate law. The overall rate may not have proportionality with the concentration in the bulk solution (Ohtani 2010). For confirmation of this theoretical

assumption, the PFO models for surface reaction controlled process and IPD for diffusion controlled process should be conducted. Finally to check the kinetic correlation between adsorption processes in the dark with photocatalysis reaction process in light the Langmuir–Hinshelwood (L-H) mechanism should also be conducted.

Langmuir: $\frac{C_e}{q_e} = \frac{C_e}{q_m} + \frac{1}{q_m K_L}$, $R_L = \frac{1}{1+K_L C_o}$ (7)

Freundlich: $\log q_e = \log K_F + 1/n \log c_e$ (8)

Dubinin-Radushkevich: $\ln q_e = -\beta\varepsilon^2 + \ln q_s, \varepsilon = RT\ln\left(1 + \frac{1}{C_e}\right), E = \frac{1}{\sqrt{2\beta}}$ (9)

Temkin: $q_e = (RT/b)\ln K_T + (RT/b)\ln c_e$ (10)

Flory-Huggins: $\ln\left(\frac{\theta}{C_o}\right) = n\ln(1-\theta) + \ln K_{FH}$, $\Delta G^o = -RT\ln(k_{FH})$ (11)

Fowler-Guggenheim: $\ln\left(\frac{C_e(1-\theta)}{\theta}\right) = \frac{2w\theta}{RT} - \ln k_{FG}$ (12)

Pseudo-first-order: $\log(q_e - q_t) = \log q_e - \left(\frac{K_1}{2.303}\right)t$ (13)

Pseudo-second-order: $t/q_t = 1/k_2 q_e^2 + t/q_e$ (14)

Elovich: $q_t = (1/\beta)\ln(\alpha\beta) + (1/\beta)\ln t$ (15)

Intra-particle adsorption-diffusion: $q = K_{id}\sqrt{t} + C$ (16)

Langmuir–Hinshelwood: $\frac{C}{r} = \frac{1}{kS}c + \frac{1}{kKS}$ (17)

Where, C_o & C_e are the initial and equilibrium concentrations of MO, respectively; q_e & q_{max} are the amounts of MO accumulated per gram of TIO and its maximum uptake, respectively; K_L is the ratio of adsorption and desorption rate constant; ε is D-RK constant; q_s is saturation capacity; β is the constant related to free energy; n is the number of ions

adsorbed on the site of the catalyst; θ = [1-(C_e/C_o)] is fractional surface coverage; T is temperature (K); R is the universal gas constant (8.314 J/molK); w is the energy of interaction; k_1 is PFO rate constant; k_i is the IPD constant; c (in equation 16) is intercept give an idea about boundary layer thickness, the larger the intercept is equal to greater value of boundary layer effect; k on L-H is reaction rate constant; K is adsorption equilibrium constant; S is limiting amount of surface adsorption; and c (in equation 17) is the concentration of analyte in the bulk solution at equilibrium (Dil et al. 2017).

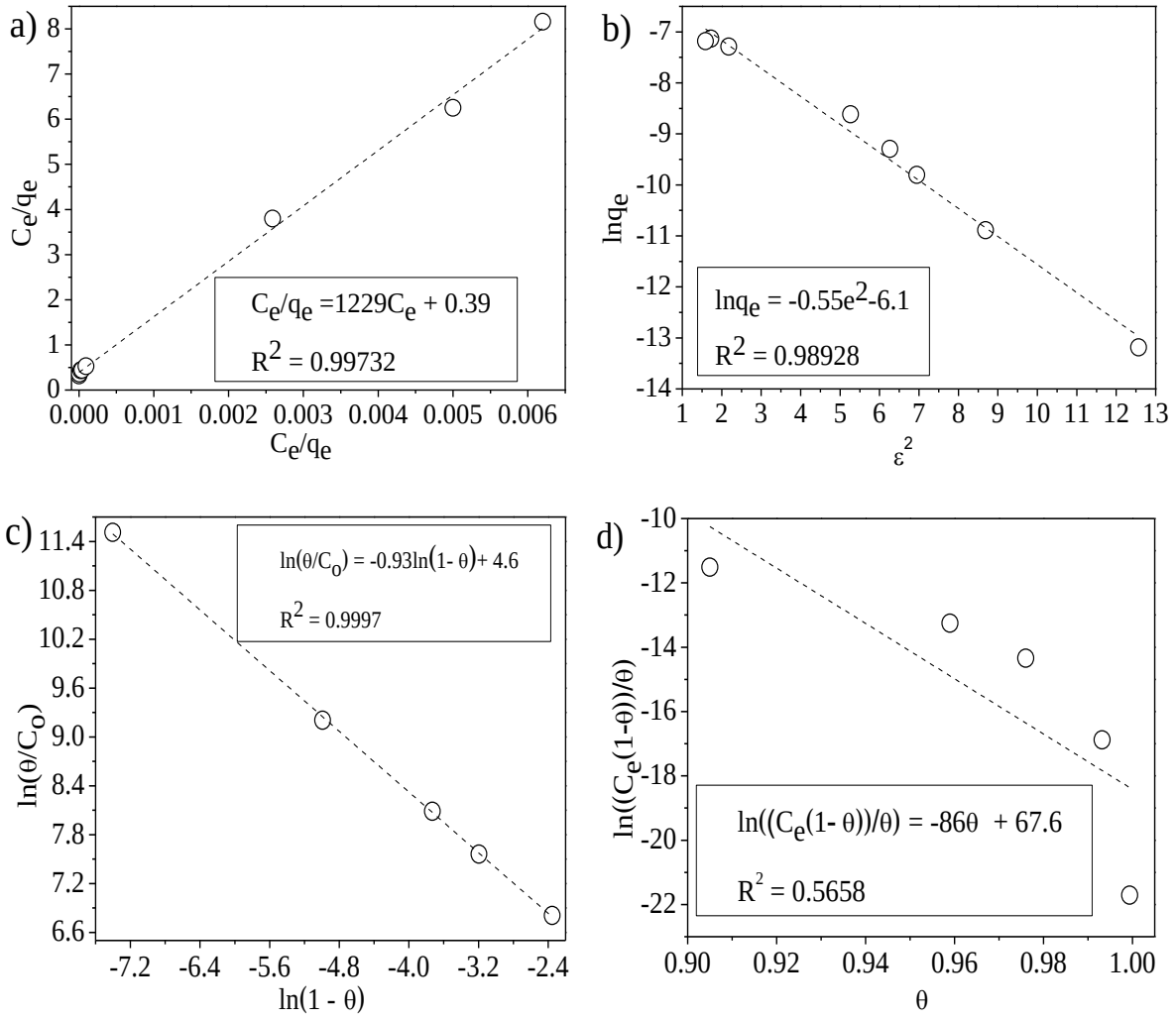

Figure 11. (a) Langmuir, (b) D-RK, (c) FH, and (d) FG adsorption isotherms of TIO-4 calcined at 500 ^oC.

The adsorption isotherm study plots of Langmuir, D-RK, FH, and FG models and their adsorption isotherm constants values are given in Figure 11a, b, c, d, and Table 3, respectively. Depending on the R^2 values (given on each plot), except FG, all the other isotherm models fit well. The essential equilibrium parameter R_L value (0.024) on Langmuir

adsorption isotherm appears in between 0 and 1 indicating the actuality of favorable adsorption. From the D-RK plots, the obtained mean adsorption energy value (0.95 kJ/mol) indicates the domination of physical adsorption as it is less than 8 kJ/mol. The negative value of free energy, ΔG (-11.40 kJ/mol) found from the FH model expresses the spontaneity of the process.

Table 3. Adsorption isotherms constant for adsorption of MO on TIOs.

Analyte	Langmuir (a)			D-RK (b)		FH (c)		FG (d)	
	q_{max}	K_L	R_L	β	E(kJ/mol)	n	ΔG(kJ/mol)	k_{FG}	w(kJ/mol)
MO	8.14 x10^{-4}	3.2 x 10^{3}	0.024	0.55	0.95	-0.93	-11.40	5 x 10^{-30}	-106.5

5.2.3. Adsorption Kinetics

As explained by Ohtani (2010), ideally the first-order kinetics works in homogenous solution. Therefore, in photocatalysis, to study the rate of reaction using first-order reaction kinetics, the reaction should be under control of the diffusion process, i.e. the rate-determining step should be adsorption of pollutant on the surface of the catalyst. On the contrary, if it is surface reaction limited, i.e. the slowest step is the reaction of e^- and h^+ with surface adsorbed MO pollutant unless it follows Henry/Langmuir-type of equations, the photocatalytic reaction rate did not obey the first-order rate law. Consequently, the overall rate did not have proportionality with the concentration in the bulk solution.

The adsorption kinetics plots of PFO, IPD in the dark and L-H plots during the photocatalytic reaction and their coefficient of determination values are given in Figure 12a, b, c, d, and Table 4, respectively. As shown in Figure 12a, the amount of adsorption increases proportionally to the time of contact up to the formation of the plateau (50 minutes). After that, due to complete coverage of the whole active sites on the surface, the adsorbed amount becomes constant. This may indicate that, for adsorption-desorption equilibration process, no need to go further above the equilibrium values of 50 minutes. From PFO plots (Figure 12b), even if the close relationship between theoretical equilibrium capacities values (9.4E-05 mol/L) with experimental data value (1.2E-04 mol/L) was detected, relative to the IPD model its R^2 value is somewhat poor. In addition, passing of the IPD linear plots through the origin, i.e. almost the intercept C is near to zero (Figure 12c), indicates the well-fitting of the model (Yang et al. 2015). Therefore, it's possible to conclude that the reaction is reasonably under control of the diffusion process.

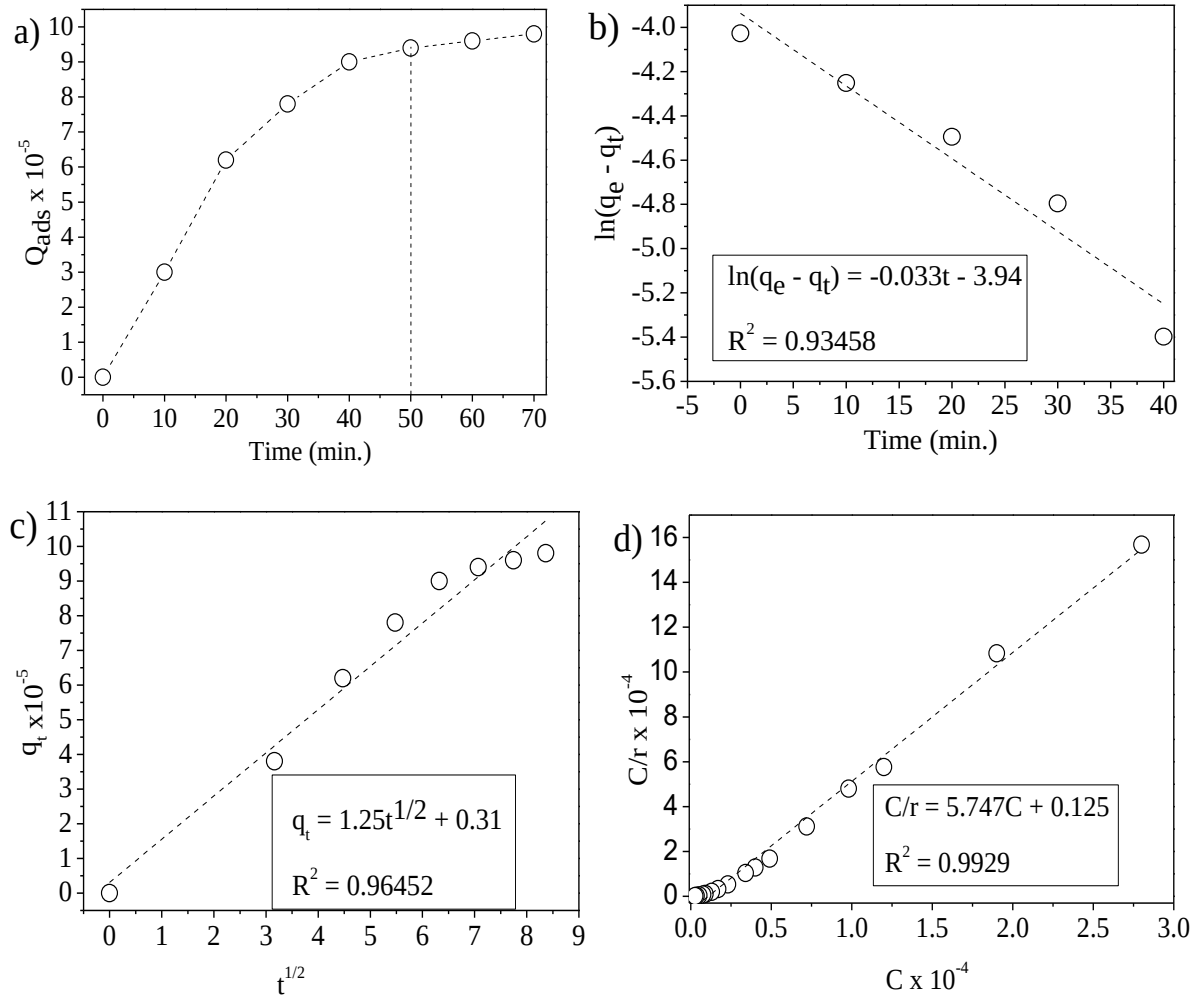

Figure 12. (a) Adsorption kinetics, (b) PFO, (c) IPD, and (d) L-H adsorption kinetics models of TIO-4 calcined at 500 ^{o}C.

Table 4. The kinetics constants and coefficient values of adsorption and degradation of MO on TIO.

Analyte	PFO				IPD			L-H	
	q_{e*}	K_1	q_e	R^2	k_{dif}	R^2	C	kS	K
MO	9.4E-05	0.076	1.2E-04	0.9346	1.25	0.9452	0.31	0.174	0.023

The two important concepts on L-H plots (Figure 13d) are (i) the well-fitting of the Langmuir type linear plots and (ii) the relation between adsorption equilibrium constant obtained during the dark and constant obtained during the photocatalytic reaction. The obtained plot confirms that the Langmuir type linear plots fit well with the data, however comparing the two constants obtained from the dark and during degradation (Table 4) poor relationship was observed. In such a case, the L-H mechanism may not be approved.

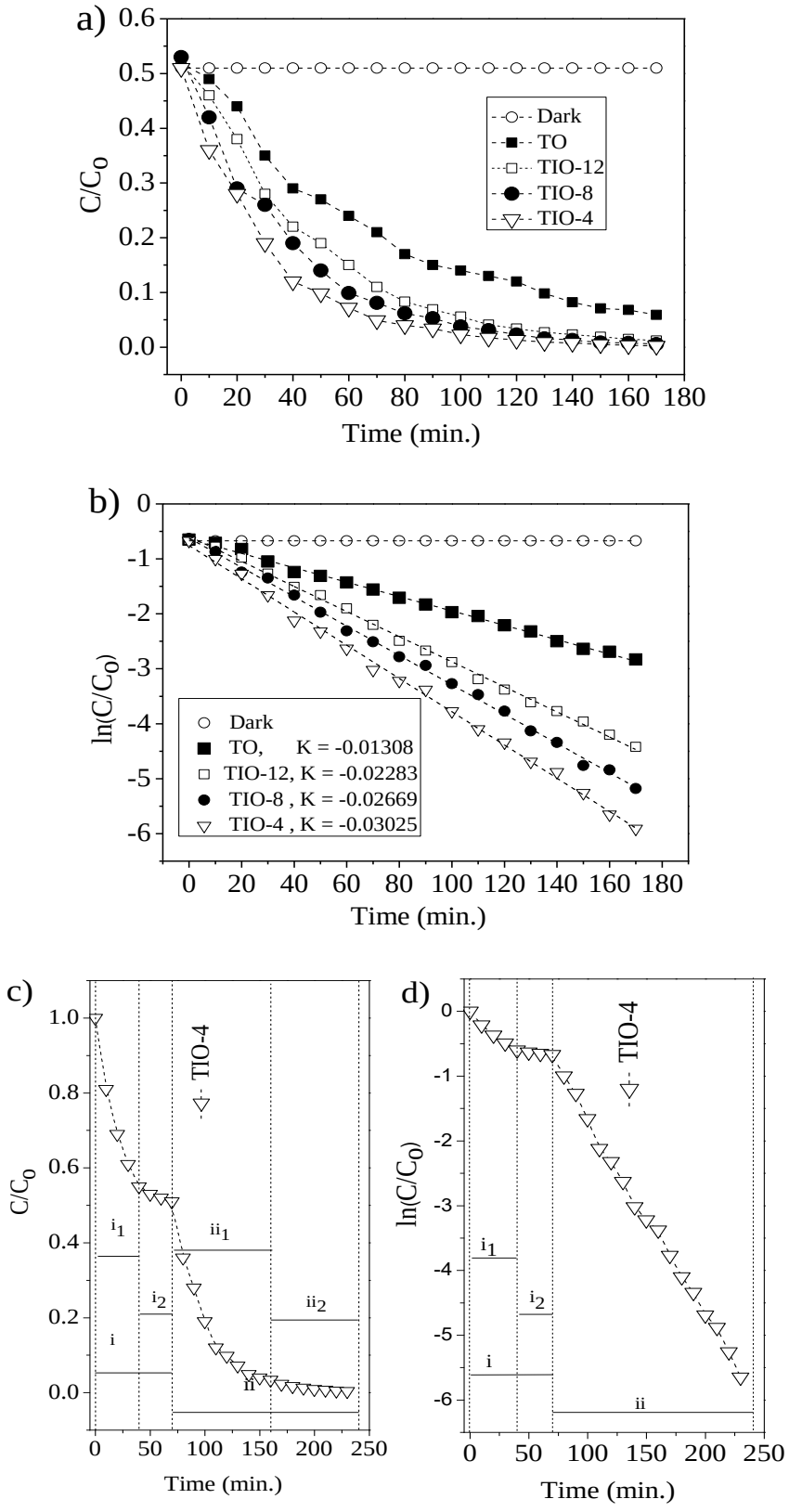

Figure 13. (a) C_o/C_t vs. t, (b) $Ln(C_o/C_t)$ vs. t, (c) C_o/C_t vs. t. and (d) Ln (C_o/C_t) vs. t for both adsorption in the dark and photocatalytic degradation in light for TIO-4 calcined at 500 ^oC.

The result in Figure 13a shows that relative to the other TIOs, TIOs-4 has the highest photocatalytic activity. This indicates that the percentage of α-Fe_2O_3 is affecting the photocatalytic activity of the synthesized materials. However, all three composites have their own activity towards the degradation of MO. As revealed on Ln (C_o/C_t) versus t plot (Figure 13b), the obtained equilibrium constant value for TIO-4 is higher compared to other TIOs. At the end of the fastest step, the experimental result indicates that almost 97 % (at 90 minutes) of MO was degraded. Therefore, after that point, it may not essential to continue the photocatalytic reaction process. Furthermore, as suggested by Bendjabeur et al. (2017), on the combined adsorption-photocatalysis plot of Figure 13c, kinetically, both the fastest (i_1& ii_1) and the slowest (i_2 & ii_2) step process for the respective adsorption (i) and photocatalysis (ii) reactions were detected.

5.3. Comparison with Related Work

Comparing with different related works (Table 5), the photocatalytic efficiency of this work appears to be much successful. In fact, the presence of different conditions that control the photocatalytic efficiency including method selection, precursor type, the behavior of pollutants, etc., makes it difficult to compare this work with those presented in Table 5. However, comparing parameters like kinetics constant k, this work exhibited fairly good efficiency.

Table 5. Short review on related works

Method	Pollutant	Precursor used		Properties		Kinetics		Ref.
		Ti	Fe	S_{BET}, $p_{v,}$ P_d	D, SEM/TEM, DRS	t (time)	K (min^{-1})	
Sol-Gel	Sulfamethazine	$C_{12}H_{28}O_4Ti$	-	166, 0.3, 6.8	10, spherical, 2.92	300	0.017	(Mendiola-Alvarez et al. 2019)
Facile impregnation	Acetaldehyde and o-xylene	TiO_2	$Fe(NO_3)_3{\cdot}9H_2O$		-, aggregated, - reshift	150	-	(Dai et al. 2019)
Wet-impregnation	Methyl orange & metribuzin	$Ti(O(CH_2)_3CH_3)_4$	$Fe(NO_3)_3{\cdot}9H_2O$	67, 0.16, 10.3	-, -, 2.41	60	0.077	(Sun et al. 2018)
Nanocasting & impregnation	Remazol brilliant red X-3BS	C16H36O4Ti	$Fe(NO_3)_3$	60.4, -, -	-, irregular, 2.59	120	0.018	(Singh et al. 2019)
-	Methyl orange	$Ti(BuO)_4$	$FeCl_3{\cdot}6H_2O$,	151, 0.2, 5.8	20, core-shell, -	75	0.059	(Fu et al. 2018)
Acidolysis-Hydrothermal	Rhodamine B	Ti-bearing tailings	$Fe(NO_3)_3{\cdot}9H_2O$	81.2, -, -	20, oblong, 2.91	160	0.075	(Sui et al. 2018)
Co-precipitation	Vibrio fischeri	$TiCl_4$	$Fe(NO_3)_3{\cdot}9H_2O$	128, -, -	10, -, 2.9	240	-	(Baniamerian et al. 2018)
Mechanical process	Methylene blue	TiO_2	Fe_3O_4	-	100-200, -, -	80	0.013	(Cheng et al. 2017)
Gaseous detonation	Methyl orange	$TiCl_4$	ferrocene	-	30, spherical, 2.59	25	0.142	(Wu et al. 2017)
Impregnation	Diazinon	TiO_2	Fe $(NO_3)_3.9H_2O$		17, round	45		(Mirmasoomi et al. 2017)
Mechanochemical	Paracetamol over	TiO_2	Fe_2O_3	58, 0.3, 18	23, irregular, 2.95	180	0.009	(Subramonian et al. 2017b)
Sol-Gel	Paracetamol	TiO2	$FeCl_3$	70, 0.2, 9.5	20, flower-like	90	0.015	(Abdel-Wahab et al. 2017)
Sol–gel	Methylene blue	$TiOCl_2$	$FeCl_2.4H_2O$ and $FeCl_3.6H_2O$	59, 0.10, 6.5	-, fine granular, 1.73	110	0.016	(Abbas et al. 2016)
Solvothermal	Rhodamine B	Tetrabutyltitanate	ferric chloride	97, 0.21, 8.7	10, spherical, -	150		(Wang et al. 2014)
sol–gel	Reactive Blue 4	$Ti(OC(CH_3)_3)_4$	$Fe(NO_3)_3.9H_2O$	74, 0.2, 8	21, spherical, -	60	0.061	(Jamalluddin and Abdullah 2011)
Impregnation	Methyl orange	TiO_2	$Fe(NO_3)_3.9H_2O$	72, 0.08, 2.4	-, Irregular, 2.59	160	0.0302	This work

S_{BET}: Specific surface area (m^2/g), $p_{V:}$ pore volume (cm^3/g), P_d: pore diameter (nm); D: crystallite size (nm); t: reaction time of irradiation (min.)

5.4. Proposed Possible Mechanisms

Since the band edges of metal oxides are dependent on surface charge, instead of deciding the mechanism of the formation of heterojunction between metal oxides only depending on literature review, conducting different analytical techniques such as photoelectrochemical, spectroelectrochemical, and electrochemical is the requirement (Beranek 2011). Depending on key points and papers that give a clue the proposed possible mechanisms for this work were given in Figure 20. As usual after adsorption of pollutants on the active sites of the TIOs photocatalyst, interaction of light ($h\boldsymbol{\nu}$) with it generates e^- and h^+ on the respective, CB and VB bands of the photocatalyst. Due to the interaction of those e^- and h^+ with other species like water and oxygen, the strong oxidizing agents i.e. hydroxyl radicals ($OH^\bullet$) will be produced (depending on the reduction and oxidation potential of the photocatalyst). Consequently, the created $OH^\bullet$ leads to mineralization of pollutant to nontoxic CO_2, H_2O and mineral acid by-products (Fig. 8a).

As suggested by Herrmann (2010), these curved arrows seem to indicate escaping of the excited species from the surface to the bulk solution phase. However, for now, instead of modifying the plot, we inform that the arrows are simply to show the reaction what is going on there, and all those reaction processes are taking place on the surface of the catalyst. To have all the above efficient processes, wise junction procedure between metal oxides must be developed. Among the three main electronic arrangements of the semiconductor metal oxide heterojunction (Fig. 8b), the staggered gap type is recommended as a precise junction for e^- - h^+ recombination hindrance.

However, as explained by Lin et al. (2015), during interaction of those oxides most probably the straddling energy band structure will form and during applying UV light, a mismatch will the result, and the combination of the two acts as the same bandgap like that of Fe_2O_3, that leads to e^- - h^+ recombination process. To prevent this, matching the band gaps of TiO_2 with Fe_2O_3 must be the crucial mechanism. As suggested by Abdullah Mirzaie et al. (2012), this matching clarified in terms of ionic bond strength between metal ions and oxygen. The electronegativity values of Ti, Fe, and O are 1.54, 1.8, and 3.4, respectively. Therefore, the order of ionic nature becomes the inverse of electronegativity; consequently the difference in energy levels between main components of CB s state and VB of O 2P becomes in the order of Ti > Fe > O.

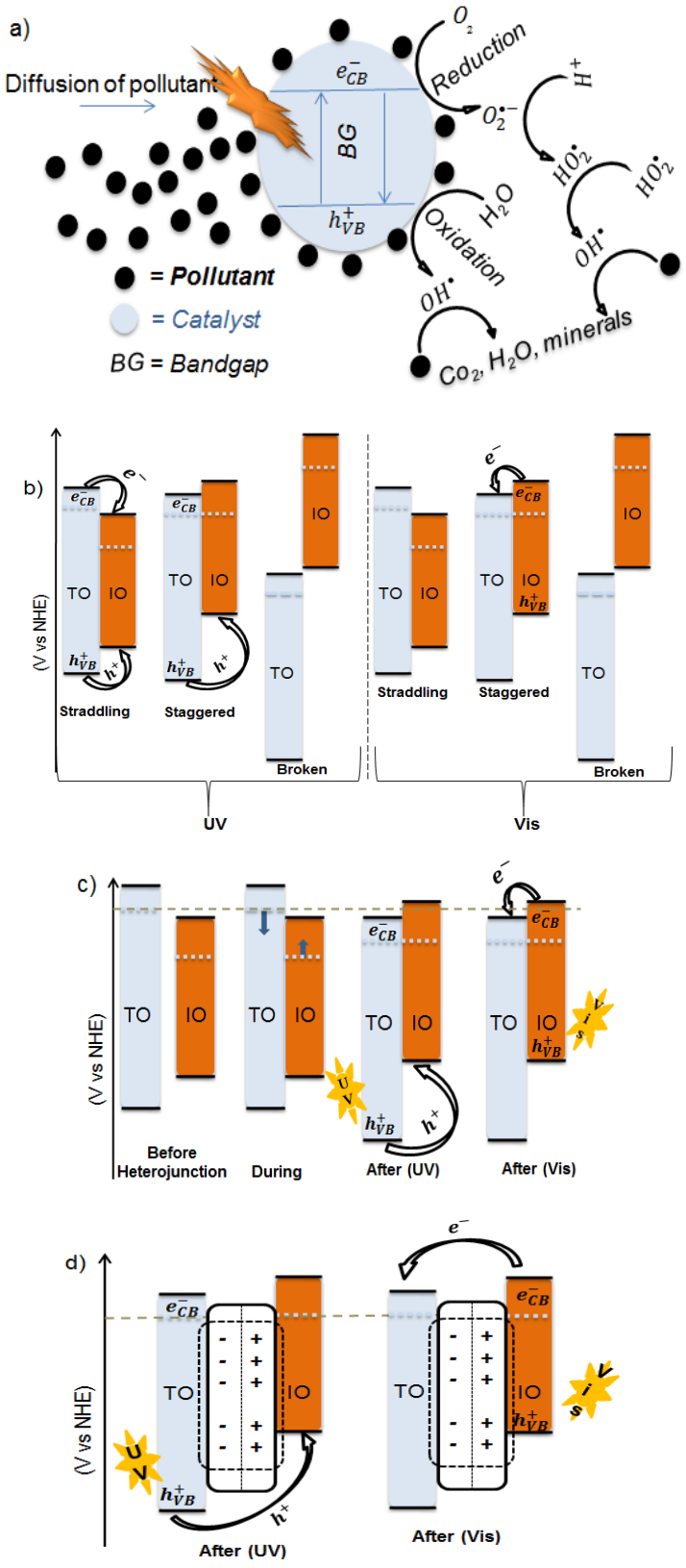

Figure 14. (a) Photocatalysis mechanism, (b) the three main electronic arrangements of semiconductor, (c) up and down movement of the Fermi level after contact, (d) the formed depletion layer that produces an electric field; TO = TiO_2 and IO = Fe_2O_3.

Furthermore, as suggested by Lachheb et al. (2017) due to the higher charge carrier concentration of TiO_2, the conduction band and Fermi level (FL) in Fe_2O_3 is larger than that in TiO_2. Therefore, as shown in Fig. 8c during heterojunction when the FL of one n-type TiO_2 semiconductor core is in contact with the FL of the other Fe_2O_3 n-type, by the movement of the FL up and down the depletion layer that produces electric field will created (Fig. 8d). The activated electric field drives the diffusion of the photogenerated e^- & h^+ out of the depletion layer and results in activation of the photocatalysis process.

6. Results and Discussion for Adsorption of Lead Ion

6.1. Characterization

6.1.1. XRD pattern

Figure 15a shows the XRD diffraction spectra of TiO_2, TIO and α-Fe_2O_3. The sharpness of the peak on TiO_2 and TIO shows its crystallinity. The particle size was calculated using the Debye Scherrer equation, $D = K\lambda/\beta cos\theta$, where d is the mean size, K is constant (0.9), λ is wavelength of x-ray (0.15506nm), β is line of broadening (in radian) and θ is Bragg angle, β = G – g; were G is the line width (in radians) and g is instrument line broadening (in radians) (Saravanan et al. 2018) . Among the various percentages of α-Fe_2O_3 impregnated into TiO_2 lattice (Figure 15b), the optimized particle size value was approximately found to be 31 nm (table 6). The effects of α-Fe_2O_3 loading were investigated as shown in table 6. The outcome revealed that on increasing loading of α-Fe_2O_3 causes decreasing the particle size and then it increases further increasing the percentage of iron oxide.

In comparison with separate titanium oxide peak and reported result of pure titania spectra, 2θ corresponding to 23.5(101), 37.1(103), 38.2(004), 38.8(102), 48.4(200), 54.40(105), 55.5(211), 67.1(116), 69.1(220) was for anatase and the other 26.0(110), 34.2(101), 43.4(210), 63.2 (002) are from rutile (Saravanan et al. 2018; Wang et al. 2015) . No matching iron oxide peaks appeared in TIO diffraction spectrum. This indicates the total impregnation of a small percentage of iron oxide in the lattice of titanium oxides. As suggested by Jamalluddin and Abdullah (2011), the absence of an appearance of peaks for α-Fe_2O_3 may be due to close similarities in radii of titanium and iron ion which were 0.68 and 0.64Å, respectively, this similarity may cause substitution of one ion by the other. The other reason for the absence of iron peak may be due to its small percentage relative to titanium oxides (Ahmed et al. 2013). In fact, that the obtained XRD pattern result for adsorption of lead ion and adsorption-photocatalysis is different. This is most probably due to different commercially available TiO_2 nanopowder used during synthesis. Furthermore, the presence of Iron oxide is also not detected on the XRD patterns of TIO material synthesized for lead ion adsorption. This is most probably, due to the small parameter shift on the synthesis procedure.

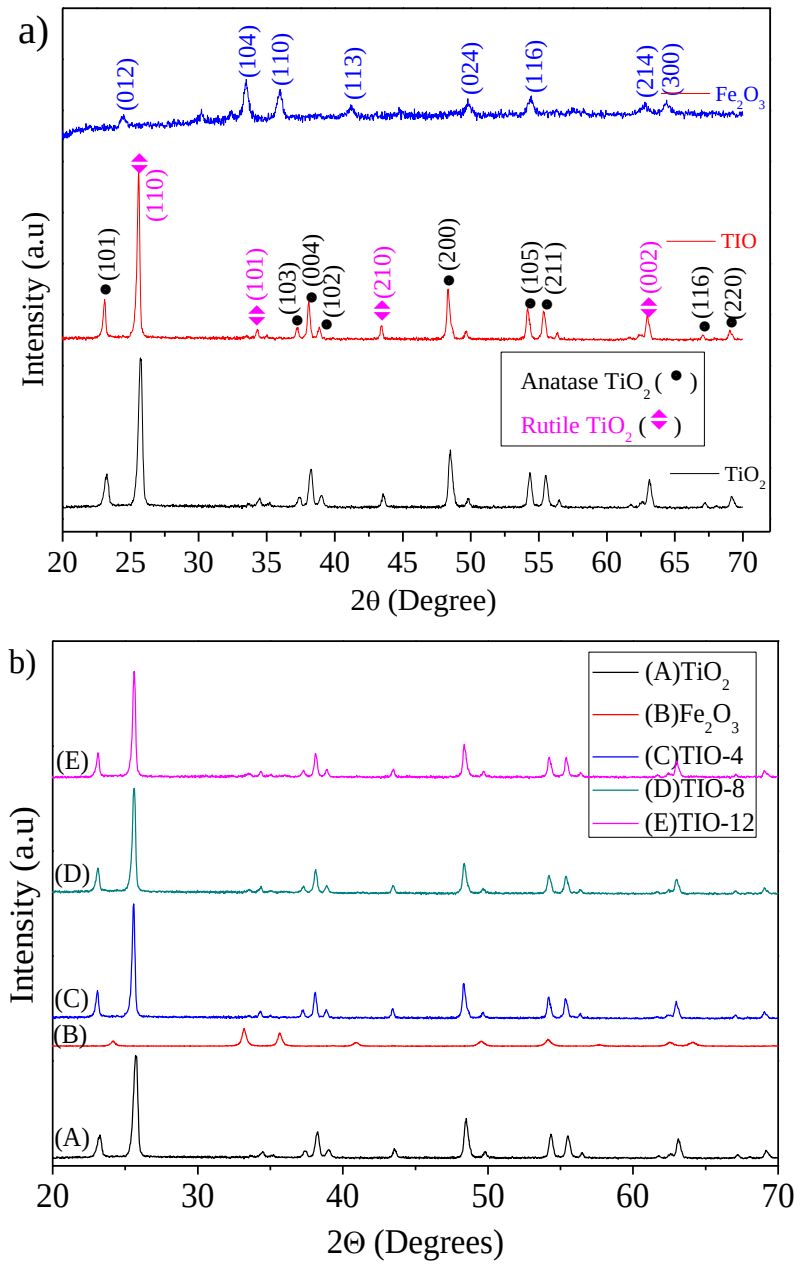

Figure 15. (a) XRD Patterns of TiO_2, α-Fe_2O_3, and TIO-4. (b) XRD Patterns of TiO_2, α-Fe_2O_3, and the three composite calcined at a temperature of 450 ^oC.

Table 6. Description of percentage composition and XRD results of the as-synthesized powders.

TiO_2 (%)	Fe_2O_3 (%)	2θ(degree)	β(degree)	θ(radian)	D(nm)
100	0	25.713	0.3542	0.2244	24.05
96	4	25.567	0.2509	0.2237	33.93
92	8	25.598	0.2758	0.2240	30.87
88	12	25.607	0.2520	0.2241	33.79
0	100	33.476	0.5237	0.2921	16.56

6.1.2. TGA-DTA analysis

From the Thermogravimetric – differentialthermal analysis (TGA-DTA) graph (Figure 16) initially due to the removal of the surface deposited moisture or solvent molecules on the powder a little weight loss was observed in between 0 to 110^{o}C. The other weight loss occurred in between 200 to 250^{o}C is probably due to the breakdown of metal hydroxide bonds of $Fe(OH)_2$. Out of 11.886mg total weight, the loss is only 0.317 mg (2.667%). Above the temperature of 380^{o}C no weight loss occurred, this indicates that the thermal stability of the metal oxides quite stable up to 1000^{o}C (Al-Hada et al. 2016). In fact, oxides may undergo phase transitions which are not simply seen by TGA.

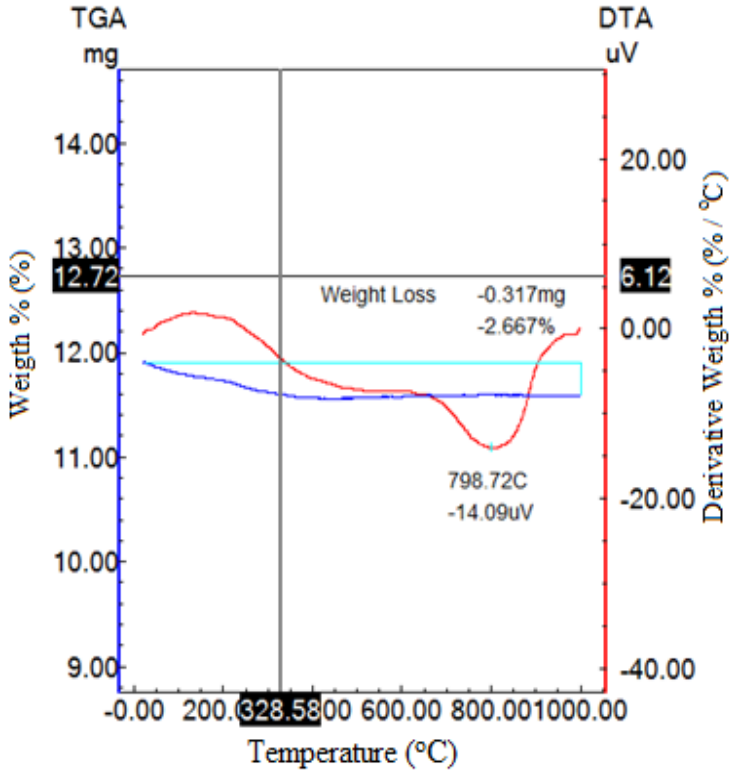

Figure 16. Thermogravimetric – differentialthermal analysis spectra of TIO-4 calcined at a temperature of 450 ^{o}C.

6.1.3. FT-IR analysis

By taking into consideration the significant peaks of inorganic materials detected below 1000 cm^{-1} on FT-IR spectra (Figure 17a). From FT- IR spectra, the band appeared at 680 cm^{-1} was due to bending vibration of Ti-O and the broadband stretched from 500 - 700 cm^{-1} was due to Ti-O-Ti and Ti-O bending vibration and on the pure iron oxide FR-IR spectra the two sharp band appeared at 540 and 465 is due to bending vibrations of Fe-O bond from iron oxide. In fact, the numbers of bands are dependent on the chemical composition, morphology, and crystal structure of the materials. If the morphology of the materials changed from zero

dimension to one, two or three dimensional morphology, the broadness and splitting also increase (Fatehah et al. 2014; Sigoli et al. 1997).

Except, some small shifts and decreasing of bands on the spectra of TIO, both TO and TIO spectra is almost similar, this indicates that the well impregnation of α-Fe_2O_3 in TiO_2 lattice. In fact, the linking of those two oxides was well confirmed by SEM-EDX analysis. The broad and strong absorption band appeared around 3426 cm^{-1} and medium band at 1613 cm^{-1} is attributed to stretching vibration of hydroxyl (O-H) and water (H-O-H) groups absorbed on the adsorbent surface, respectively. Those bands are common on metal oxides and very essential for adsorption process (Abbas et al. 2016; Subramonian et al. 2017a).

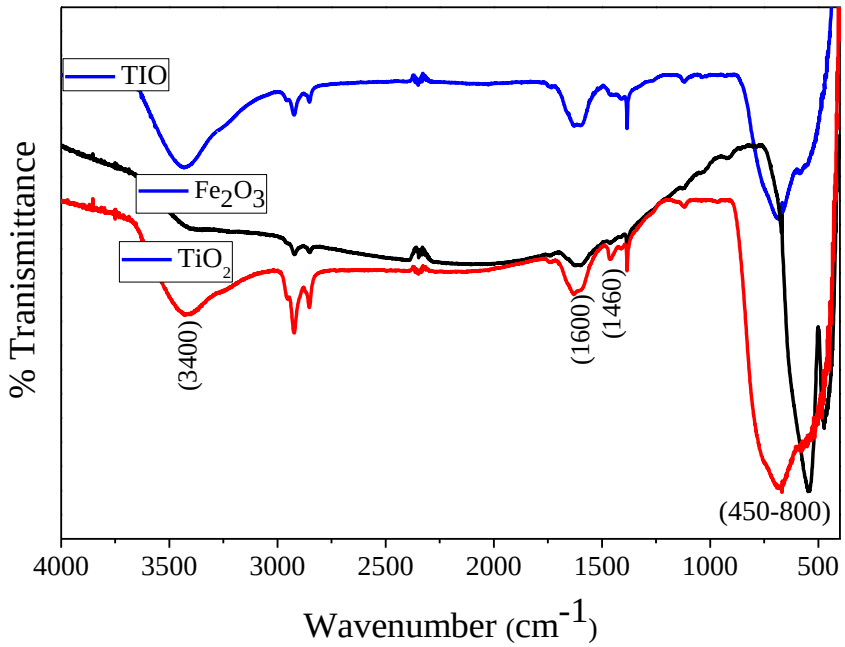

Figure 17. FT-IR spectra of TiO_2, Fe_2O_3, and TIO-4 calcined at a temperature of 450 ^oC.

6.1.4. Morphology study

From the SEM-EDX spectrum of Ti-Fe oxide (Figure 18) when we see the deeply spherical shape of nearly equal size were observed. The EDXS spectrum confirms only the presence of Fe, Ti, C and O. The appearance of carbon (C) is from the standard used during analysis. The appearance of only the three elements without any other elements indicates the purity of the powder.

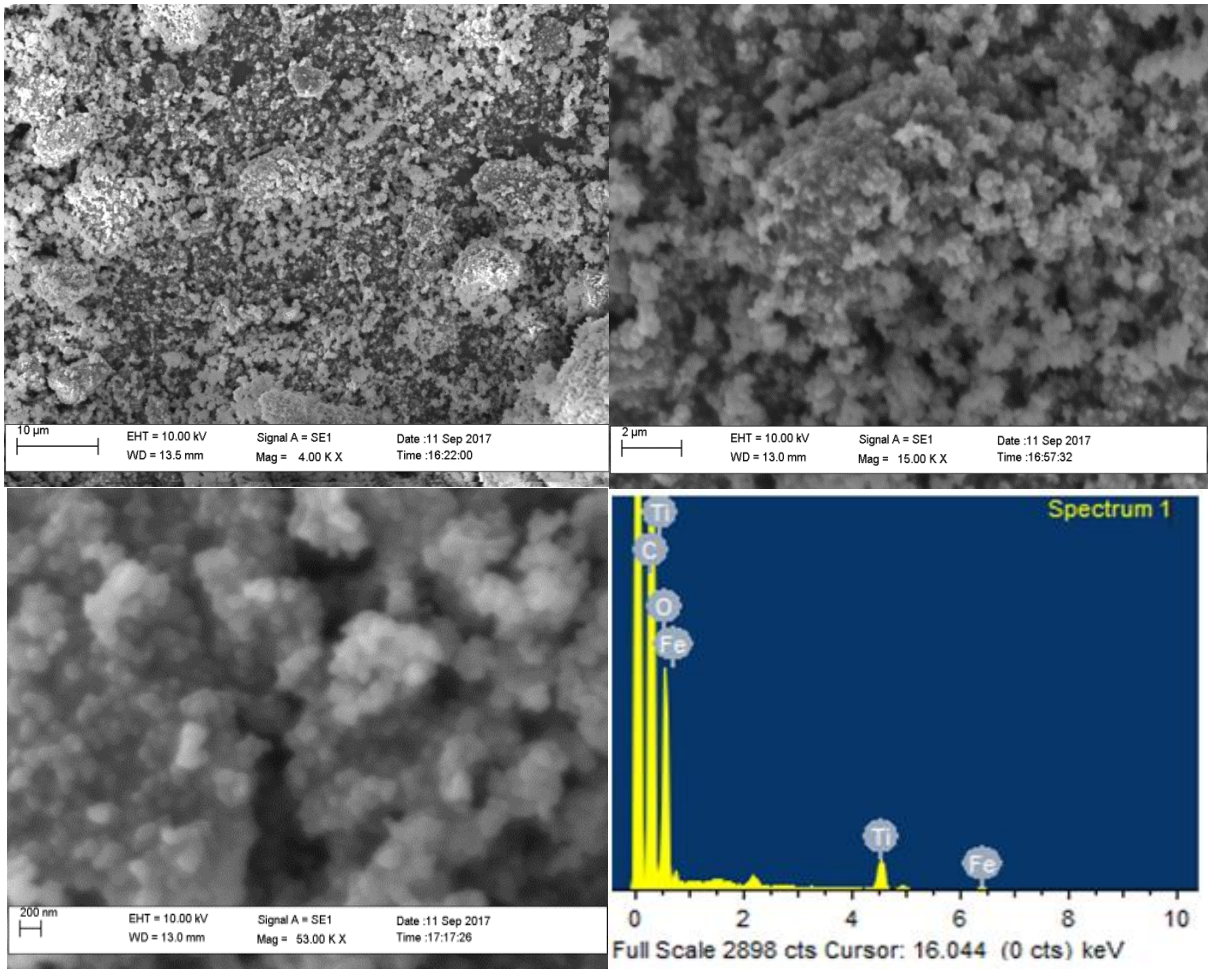

Figure 18. SEM images with different magnification and EDX spectra of TIO-4 calcined at a temperature of 450 ^{o}C.

6.2. Adsorption Study

6.2.1. Optimization

The effects of solution pH, dose, agitation speed, and time of contact for sorption of lead ion were conducted (Figure 19). During pH optimization, the greatest sorption was observed under alkaline pH range (Figure 19a). Due to H^{+}, the acidic pH makes the surface of metal oxides to be more positive, so repulsive interaction exists between the oxides and lead cation. Above seven pH value, the presence of OH^{-} assists the surface to be more negatively charged, therefore, the interactions become attractive (Ofomaja et al. 2010). On dosage optimization (Figure 19b), up to the optimum point (0.1g), the sorption efficiency was found to be high which is due to the availabilities of high sorption sites (Liu et al. 2015). But, further increasing adsorbent dosage, it does not show significant change, because, the total number of the adsorbate become negligible.

From Figure 19c as the speed of agitation increases, diffusion of lead ion towards the adsorbent surface also increases. After the optima (100 rpm) as the rate of agitation speed further increases the adsorbate starts to desorb from the surface. And on contact time optimization (Figure 19d), after reaching an optimum point 130 min., sorption capacity becomes constant since the sorbent sites were almost occupied.

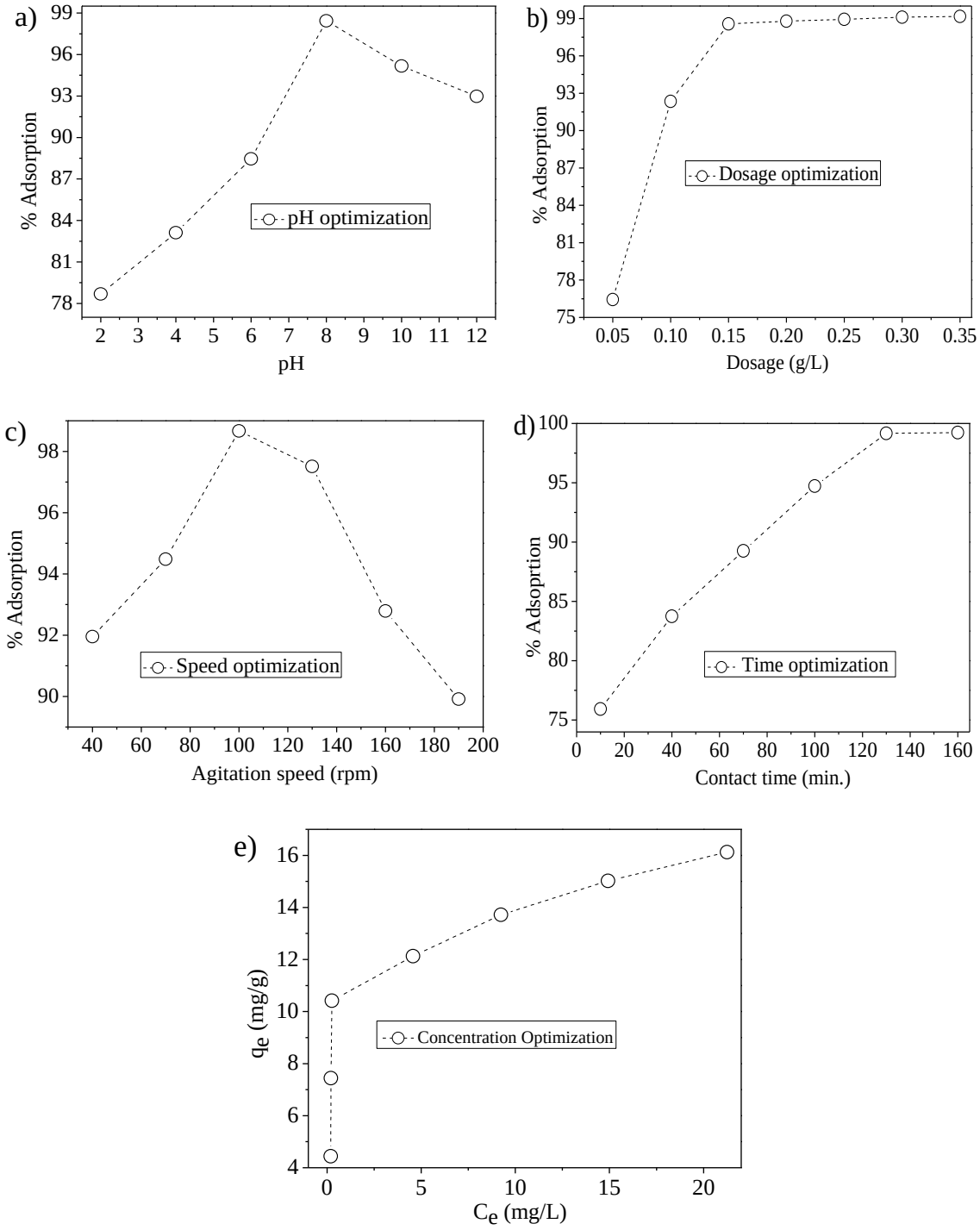

Figure 19. Effect of (a) pH, (b) adsorbent dose, (c) agitation speed, (d) contact time, (e) adsorption isotherm for lead ion adsorption on to TIO-4 calcined at a temperature of 450 ^{o}C.

6.2.3. Adsorption isotherms

The experimental data conducted by taking different initial concentration (Figure 19e) were fitted by Langmuir, Freundlich, Fowler-Guggenheim (FG), Flory-Huggins (FH), Temkin and Dubinin-Radushkevich (D-RK) isotherm models. Figure 20a - f explains the sorption isothermal behavior based on concentration optimization results. The extracted sorption constant values are given in Table 7.

Table 7. kinetics constants for sorption of lead ion on the binary oxide.

	Langmuir		Freundlich		Fowler-Guggenheim		Dubinin-Radushkevich		Temkin		Flory-Huggins	
q_{max}	*b*	R_L	k_f	*n*	k_{FG}	*w(kJ/mol)*	*E(kJ/mol)*	*β*	*b(J/mol)*	k_T	*n*	*ΔG(kJ/mol)*
16.67	1.3	0.02	10.21	6.71	$4.2*10^{-9}$	-25.7	3.45	-0.042	1293	202.5	-0.363	-12.137

Depending on R^2 values (given on each graph) Langmuir sorption isotherm model (Figure 20a) fits the sorption data relatively better than other models. The R_L value tells the type of isotherm to be unfavorable ($R_L > 1$), linear (= 1), irreversible (= 0) and favorable (< 1). The R_L values in this study were in between 0 and 1 indicating that the adsorption is favorable. The Freundlich isotherm model (Figure 20b), which is responsible for the heterogeneity of the adsorbent sites. Generally if the value of constant, n is in between 1 and 10, the adsorption process becomes acceptable and when the value of n is greater than one, physical adsorption process occurs and if it's less than one the adsorption process become chemically driven. The value of n obtained for this study was 6.71, which shows that the domination of the physical adsorption process and also indicates the presence of high affinity between adsorbate and absorbent.

From FG (Figure 20c) model which accounts the surface characteristics of adsorbate adsorbed on the adsorbent, being the value of heat of adsorption (*w*) negative (-25.7 $KJmol^{-1}$) indicates the presence of repulsive interaction between adsorbed molecules. D-RK (Figure 20d) and FH (Figure 20e) models fits relatively less, this may be because of those model are suitable for only intermediate adsorbate concentration range. As reported by Dil et al. (2017) on D-RK isotherm model, if the mean free energy, E < 8kJ/mol indicates the domination of physical adsorption, 8 – 16 kJ/mol (ion exchange) and 20 - 40$KJ \cdot mol^{-1}$ (chemical adsorption). The obtained mean free energy, E value for this study was 3.45kJ/mol, and this indicates that the physical adsorption is the controlling mechanism.

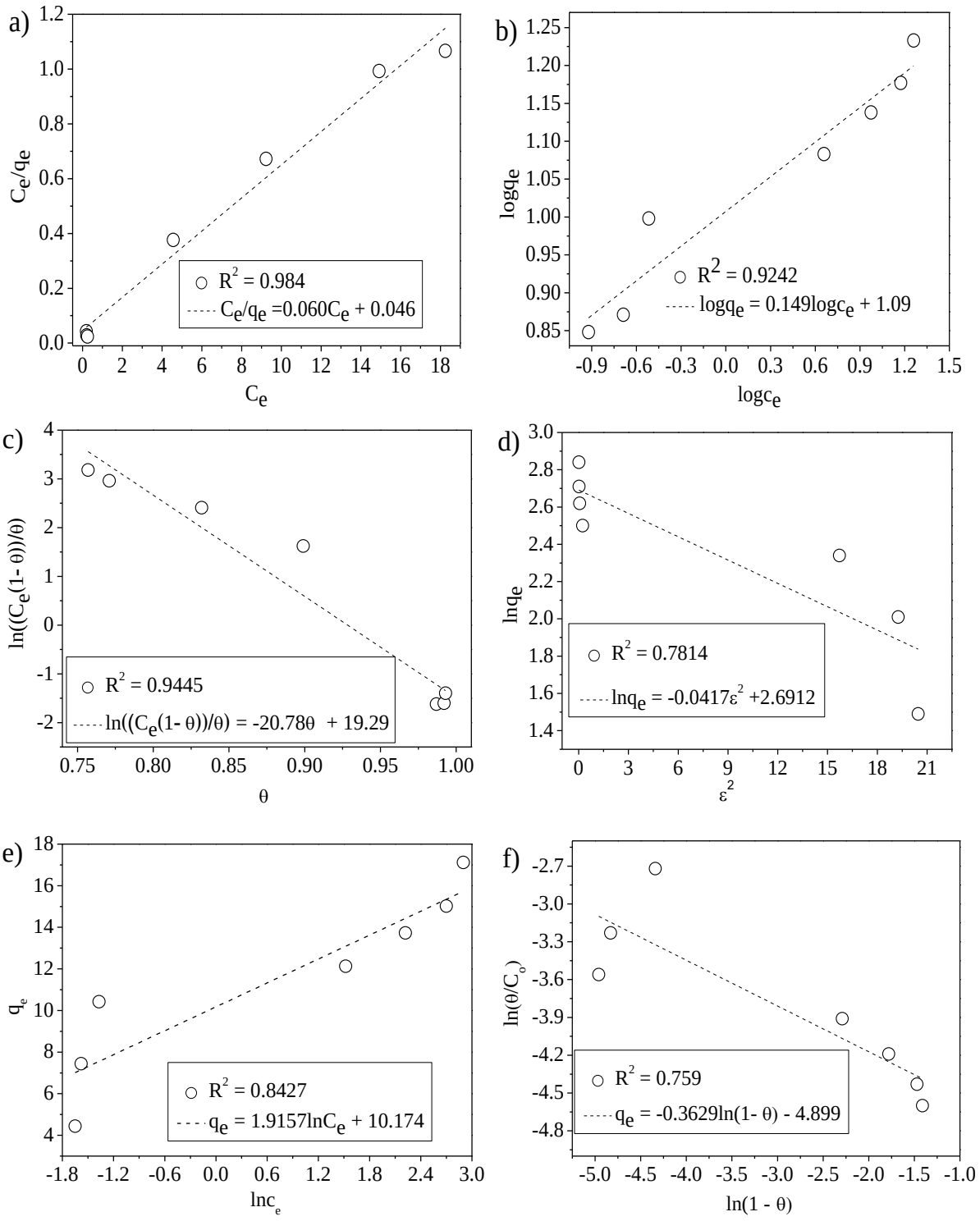

Figure 20. (a) Langmuir, (b) Freundlich, (c) Fowler-Guggenheim, (d) Dubinin-Radushkevich, (e) Temkin and (f) Flory-Huggins adsorption isotherm of Pb^{+2} on TIO-4 calcined at a temperature of 450 ^{o}C.

The Temkin model (Figure 20e) which is valid only for an intermediate range of adsorbate concentrations and gives information for adsorbate/adsorbate interactions. The constant K_T

(202.5 Lg^{-1}) on Temkin is equilibrium binding constant which is related to maximum bonding energy. The FH model (Figure 20f) which is responsible for characteristic surface coverage of the adsorbate adsorbed on the adsorbent and responsible for suggesting the spontaneity of the reaction. The obtained values of standard free energy (ΔG^o) from the FH model was -12.14kJ/mol, this value indicates that the reaction was spontaneous. The obtained maximum uptake corresponding to the site saturation (q_{max}) for the adsorbent is 16.67mg/g.

6.2.4. Kinetics of adsorption

The results of the kinetics of sorption study obtained after optimization of all parameters are shown in Figure 21.

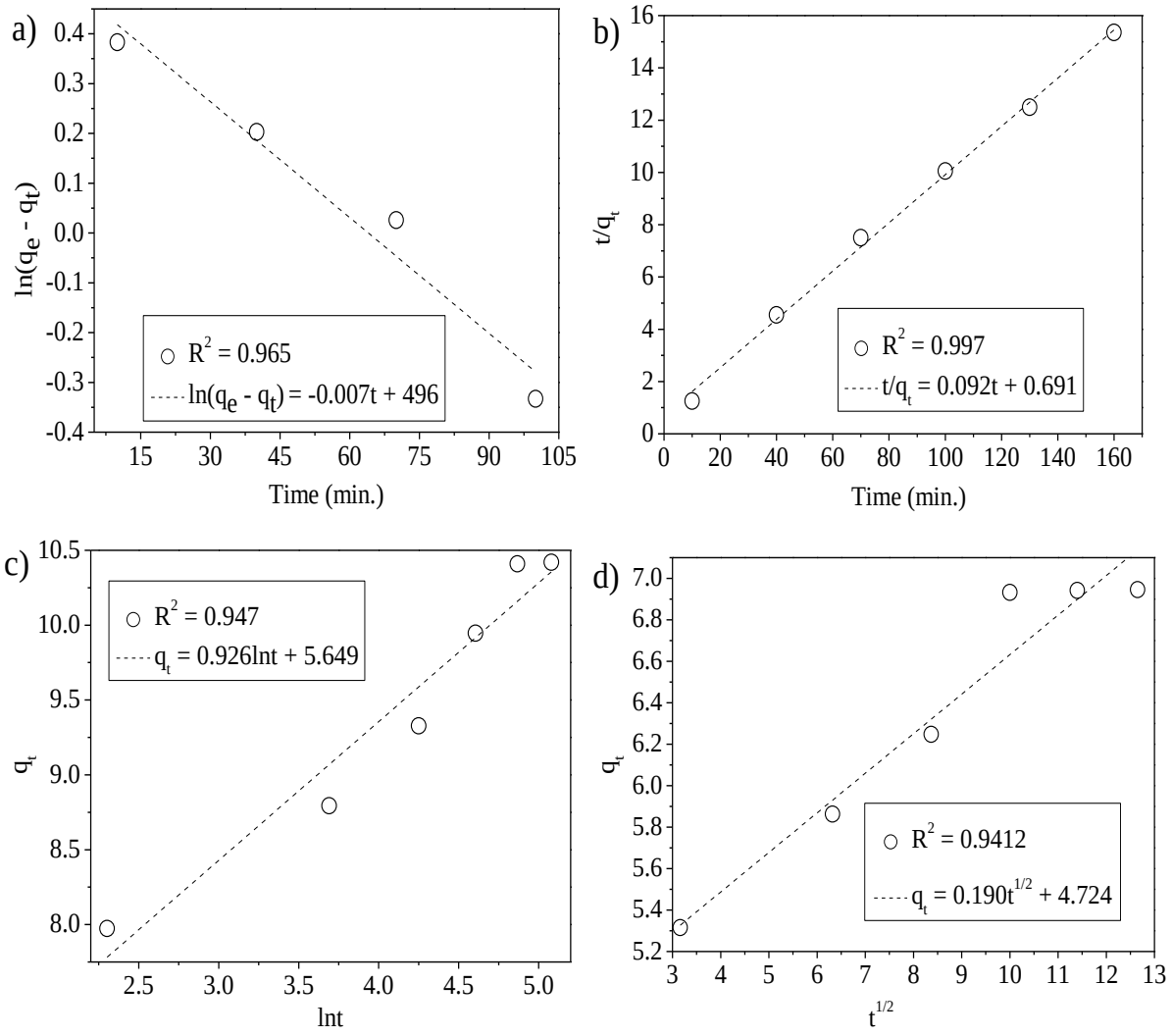

Figure 21. Plot of (a) pseudo-first order, (b) pseudo-second order, (c) Elovich and (d) intra-particle diffusion model of Pb^{+2} on TIO-4 calcined at a temperature of 450 ^oC.

From adsorption-reaction models: PFO (Figure 21a), PSO (Figure 21b) and Elovich (Figure 21c) were tested. Depending on R^2 values PSO model relatively fits well than PFO and Elovich and its theoretical equilibrium capacity values (10.41 mg/g) also fits well with experimental data values (10.87 mg/g) (Alipanahpour Dil et al. 2017).

Being the R^2 values for IPD is relatively less than other adsorption-reaction models suggest that the mechanism is not under control of adsorption-diffusion kinetics, actually to say the reaction is under the control of diffusion kinetics, also the IPD linear line should pass through the origin(C = O), unlike that of obtained result on this paper. Therefore, possible to deduce that the reaction is totally under the control of surface/adsorption-reaction (Yang et al. 2015).

However, there is great variation between experimental (3.133 mg/g) and theoretical (10.41mg/g) values for PFO. Often the calculated q_e value is less than the experimental value, but it should be close to each other to say the model is fitted well (Das et al. 2014). The calculated results and different constants for the kinetics model were presented in Table 8. From adsorption-diffusion model which helps to check whether the reaction mechanism is under control of adsorption-diffusion in addition to surface reaction, the intraparticle diffusion (IPD) model was tested.

Table 8. kinetics constants and coefficient values of lead sorption on binary metal oxides.

Metal	Pseudo-first				Pseudo-second			IPD		Elovich model			
	q_{e*}	K_1	q_e(mg/g)	R^2	K_2	q_e(mg/g)	R^2	k_{dif}	R^2	C	β	α	R^2
Pb(II)	10.41	0.016	3.133	0.965	0.012	10.87	0.997	0.19	0.947	4.72	1.08	173	0.941

*****represents calculated q_e values

6.3. Thermodynamics Study

The effect of temperature on lead ion sorption is shown in Figure 22a. For the values of ΔG^o being negative and the values of ΔH^o being positive indicates the respective spontaneous and an endothermic reaction of sorption (Table 9). As temperature increases the ΔG^o values decrease, which shows that the sorption process of lead ion is high at high temperature. The thermodynamic parameters (ΔG, ΔH, and ΔS) can be calculated using the following equation:

$$\Delta G = -RT\ln Kc \quad (18)$$

$$\ln K_c = -\Delta H^o/RT + \Delta S^o/R \quad (19)$$

$$\Delta G^0 = \Delta H^o - T\Delta S^o \quad (20)$$

Where R (8.314 J/molK) is universal gas constant, T(K) is the absolute temperature and K_c is the standard thermodynamic equilibrium constant defined by q_e/C_e.

Table 9. Values of thermodynamic parameters for lead ion sorption.

T(K)	ΔG(KJ/mol)	ΔH(KJ/mol)	ΔS(J/molK)
298	-9.219	28.471.3	126.48
308	-10.48		
318	-11.75		
328	-13.01		

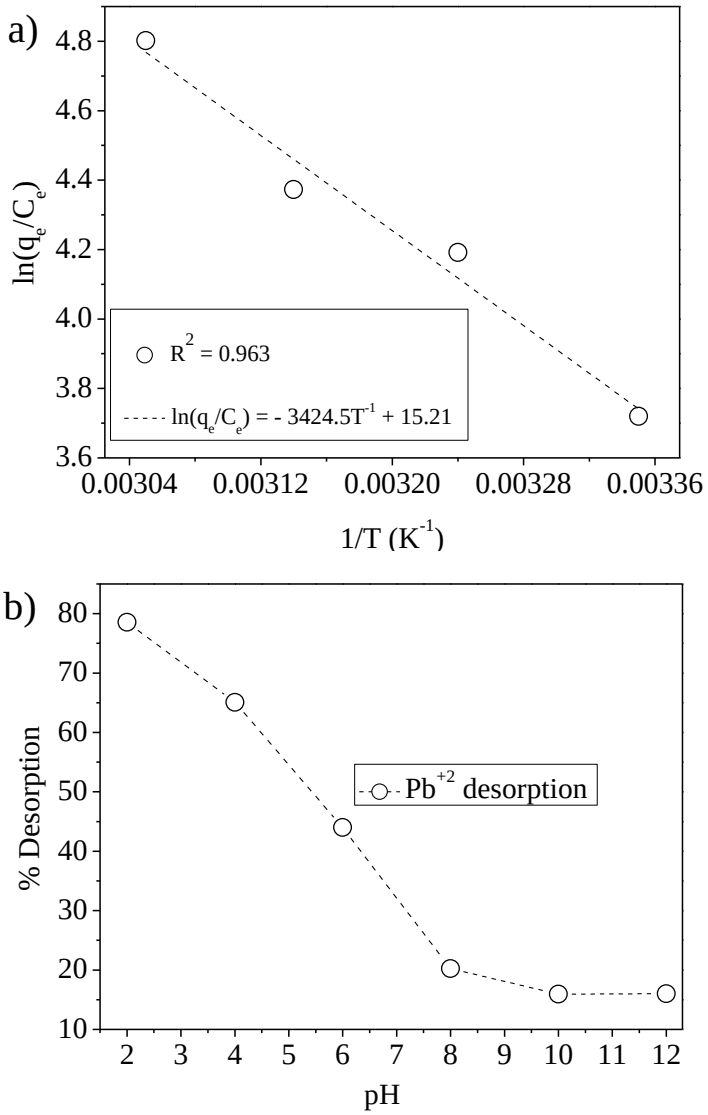

Figure 22. (a) Plot of thermodynamic study and (b) Effect of pH on desorption of lead ion on to TIO-4 at various pH values.

By plotting the graph of $\ln K_c$ versus 1/T, the value of ΔH^o and ΔS^o can be estimated from the slopes and intercept values. The decrease in ΔG^o with increasing temperature indicates more efficient sorption at a higher temperature (Alfaro-Cuevas-Villanueva et al. 2014).

6.4. Desorption Study

From the reproducibility/desorption studies (Figure 22b), as pH increases, the amount of desorption of lead ion decreases. About 79 % of adsorbed lead ions were desorbed. The desorption efficiency was calculated using the equation as given below:

$$\% \text{ Desorption efficiency} = \frac{\text{Desorbed}}{\text{Adsorbed}} * 100 \qquad (21)$$

Where desorbed is the amount of the lead ion that was removed from loaded powder after desorption study and adsorbed is $(C_o - C_e)$ for each recovery process.

7. Conclusions

For the photocatalytic study, the TIOs binary nanocomposite materials were synthesized using the solvent-free impregnation method. The good impregnation of α-Fe_2O_3 in TiO_2 lattice was confirmed by SEM-EDX image, XRD, FT-IR, and UV-Vis spectra. To do the photocatalysis experiment, since it is important to test the adsorption isotherm as well as adsorption kinetics in dark, the Langmuir, D-RK, and FH adsorption isotherm models and the PFO adsorption-reaction and IPD adsorption-diffusion kinetics models were tested. Except for FG, all the other isotherm models fit well and the obtained results prove domination of physical adsorption; and the spontaneity of the reaction. Furthermore, comparing the L-H adsorption isotherm constant value with the constant obtained in dark, different results were observed. Therefore, instead of passing only by fitting the concentration versus reaction time plot, proving and giving the adsorption isotherm values is the critical point. Among these different percentages of Fe_2O_3 (4, 8, and 12 % of α-Fe_2O_3) impregnated TiO_2 and bare TiO_2, the TIO-4 sample showed better photocatalytic activity. The obtained approximate equilibrium constant (k) value from the kinetics study was found to be 0.03025. During lead ion adsorption, factors affecting adsorption experiment (pH, adsorbent dose, speed of agitation, time of contact and initial lead ion concentration) were optimized. Compared to other adsorption isotherm models that are used for understanding of the adsorption process, the Langmuir adsorption isotherm model fits well. From PFO, FSO, and Elovich adsorption-reaction kinetics models, PSO has fitted the adsorption mechanism well. The IPD adsorption-diffusion model fails to fit well and its line also not pass through the origin. Therefore, the adsorption kinetics is under control of the adsorption-reaction mechanism. The assistance of temperature increment for adsorption of lead ion on the adsorbent and spontaneity the reaction were also proofed by thermodynamics study.

References

Abbas, N., Shao, G. N., Haider, M. S., Imran, S. M., Park, S. S., & Kim, H. T. (2016). Sol–gel synthesis of TiO2-Fe2O3 systems: Effects of Fe2O3 content and their photocatalytic properties. *Journal of Industrial and Engineering Chemistry*, *39*, 112–120. https://doi.org/10.1016/j.jiec.2016.05.015

Abdel-Wahab, A.-M., Al-Shirbini, A.-S., Mohamed, O., & Nasr, O. (2017). Photocatalytic degradation of paracetamol over magnetic flower-like Ti2/Fe2O3 core-shell nanostructures. *Journal of Photochemistry and Photobiology A: Chemistry*, *347*, 186–198. https://doi.org/10.1016/j.jphotochem.2017.07.030

Abdullah Mirzaie, R., Kamrani, F., Anaraki Firooz, A., & Khodadadi, A. A. (2012). Effect of α-Fe2O3 addition on the morphological, optical and decolorization properties of ZnO nanostructures. *Materials Chemistry and Physics*, *133*(1), 311–316. https://doi.org/10.1016/j.matchemphys.2012.01.029

Abebe, B., & Ananda Murthy, H. C. (2018). Synthesis and Characterization of Ti-Fe Oxide Nanomaterials for Lead Removal. *Journal of Nanomaterials*, *2018*, 1–10. https://doi.org/10.1155/2018/9651039

Abebe, B., Taddesse, A. M., Kebede, T., Teju, E., & Diaz, I. (2017). Fe-Al-Mn ternary oxide nanosorbent: Synthesis, characterization and phosphate sorption property. *Journal of Environmental Chemical Engineering*, *5*(2), 1330–1340. https://doi.org/10.1016/j.jece.2017.02.026

Ahmed, M. A., El-Katori, E. E., & Gharni, Z. H. (2013). Photocatalytic degradation of methylene blue dye using Fe2O3/TiO2 nanoparticles prepared by sol–gel method. *Journal of Alloys and Compounds*, *553*, 19–29. https://doi.org/10.1016/j.jallcom.2012.10.038

Ahmed, S., Rasul, M. G., Brown, R., & Hashib, M. A. (2011). Influence of parameters on the heterogeneous photocatalytic degradation of pesticides and phenolic contaminants in wastewater: A short review. *Journal of Environmental Management*, *92*(3), 311–330. https://doi.org/10.1016/j.jenvman.2010.08.028

Al-Hada, N. M., Saion, E., Kamari, H. M., Flaifel, M. H., Shaari, A. H., Talib, Z. A., et al. (2016). Structural, morphological and optical behaviour of PVP capped binary (ZnO)0.4 (CdO)0.6 nanoparticles synthesised by a facile thermal route. *Materials Science in Semiconductor Processing*, *53*, 56–65. https://doi.org/10.1016/j.mssp.2016.06.004

Alder, C. M., Hayler, J. D., Henderson, R. K., Redman, A. M., Shukla, L., Shuster, L. E., & Sneddon, H. F. (2016). Updating and further expanding GSK's solvent sustainability guide. *Green Chemistry*, *18*(13), 3879–3890. https://doi.org/10.1039/C6GC00611F

Alfaro-Cuevas-Villanueva, R., Hidalgo-Vázquez, A. R., Cortés Penagos, C. de J., & Cortés-Martínez, R. (2014). Thermodynamic, Kinetic, and Equilibrium Parameters for the Removal of Lead and Cadmium from Aqueous Solutions with Calcium Alginate Beads. *The Scientific World Journal*, *2014*, 1–9. https://doi.org/10.1155/2014/647512

Ali, I., Alharbi, O. M. L., Alothman, Z. A., & Alwarthan, A. (2018). Facile and eco-friendly synthesis of functionalized iron nanoparticles for cyanazine removal in water. *Colloids and Surfaces B: Biointerfaces*, *171*(July), 606–613.

https://doi.org/10.1016/j.colsurfb.2018.07.071

Alipanahpour Dil, E., Ghaedi, M., Ghezelbash, G. R., Asfaram, A., & Purkait, M. K. (2017). Highly efficient simultaneous biosorption of Hg2+, Pb2+ and Cu2+ by Live yeast Yarrowia lipolytica 70562 following response surface methodology optimization: Kinetic and isotherm study. *Journal of Industrial and Engineering Chemistry*, *48*, 162–172. https://doi.org/10.1016/j.jiec.2016.12.035

An, H., Zhou, J., Li, J., Zhu, B., Wang, S., Zhang, S., et al. (2009). Deposition of Pt on the stable nanotubular TiO2 and its photocatalytic performance. *Catalysis Communications*, *11*(3), 175–179. https://doi.org/10.1016/j.catcom.2009.09.020

Arslan-Alaton, I. (2003). A review of the effects of dye-assisting chemicals on advanced oxidation of reactive dyes in wastewater. *Coloration Technology*, *119*(6), 345–353. https://doi.org/10.1111/j.1478-4408.2003.tb00196.x

Baniamerian, H., Safavi, M., Alvarado-Morales, M., Tsapekos, P., Angelidaki, I., & Shokrollahzadeh, S. (2018). Photocatalytic inactivation of Vibrio fischeri using Fe2O3-TiO2-based nanoparticles. *Environmental Research*, *166*(March), 497–506. https://doi.org/10.1016/j.envres.2018.06.011

Basheer, A. A. (2018). Chemical chiral pollution: Impact on the society and science and need of the regulations in the 21st century. *Chirality*, *30*(4), 402–406. https://doi.org/10.1002/chir.22808

Bendjabeur, S., Zouaghi, R., Kaabeche, O. N. ., & Sehili, T. (2017). Parameters Affecting Adsorption and Photocatalytic Degradation Behavior of Gentian Violet under UV Irradiation with Several Kinds of TiO2 as a Photocatalyst. *International Journal of Chemical Reactor Engineering*, *15*(4). https://doi.org/10.1515/ijcre-2016-0206

Beranek, R. (2011). (Photo)electrochemical Methods for the Determination of the Band Edge Positions of TiO2-Based Nanomaterials. *Advances in Physical Chemistry*, *2011*(Iv), 1–20. https://doi.org/10.1155/2011/786759

Bizarro, M. (2010). High photocatalytic activity of ZnO and ZnO:Al nanostructured films deposited by spray pyrolysis. *Applied Catalysis B: Environmental*, *97*(1–2), 198–203. https://doi.org/10.1016/j.apcatb.2010.03.040

Boehm, H. P. (1966). Chemical Identification of Surface Groups. In *The Physics Teacher* (Vol. 14, pp. 179–274). https://doi.org/10.1016/S0360-0564(08)60354-5

Braslavsky, S. E. (2007). Glossary of terms used in photochemistry, 3rd edition (IUPAC Recommendations 2006). *Pure and Applied Chemistry*, *79*(3), 293–465. https://doi.org/10.1351/pac200779030293

Carpenter, S. R., Caraco, N. F., Correll, D. L., Howarth, R. W., Sharpley, A. N., & Smith, V. H. (1998). Nonpoint pollution of surface waters with phosphorus and nitrogen. *Ecological Applications*, *8*(3), 559–568. https://doi.org/10.1890/1051-0761(1998)008[0559:NPOSWW]2.0.CO;2

Charles, J., Bradu, C., Morin-Crini, N., Sancey, B., Winterton, P., Torri, G., et al. (2016). Pollutant removal from industrial discharge water using individual and combined effects of adsorption and ion-exchange processes: Chemical abatement. *Journal of Saudi*

Chemical Society, *20*(2), 185–194. https://doi.org/10.1016/j.jscs.2013.03.007

Chen, F., Ho, P., Ran, R., Chen, W., Si, Z., Wu, X., et al. (2017). Synergistic effect of CeO2 modified TiO2 photocatalyst on the enhancement of visible light photocatalytic performance. *Journal of Alloys and Compounds*, *714*, 560–566. https://doi.org/10.1016/j.jallcom.2017.04.138

Cheng, L., Qiu, S., Chen, J., Shao, J., & Cao, S. (2017). A practical pathway for the preparation of Fe2O3 decorated TiO2 photocatalyst with enhanced visible-light photoactivity. *Materials Chemistry and Physics*, *190*, 53–61. https://doi.org/10.1016/j.matchemphys.2017.01.001

Chong, M. N., Jin, B., Zhu, H. Y., Chow, C. W. K., & Saint, C. (2009). Application of H-titanate nanofibers for degradation of Congo Red in an annular slurry photoreactor. *Chemical Engineering Journal*, *150*(1), 49–54. https://doi.org/10.1016/j.cej.2008.12.002

Chong, M. N., Lei, S., Jin, B., Saint, C., & Chow, C. W. K. (2009). Optimisation of an annular photoreactor process for degradation of Congo Red using a newly synthesized titania impregnated kaolinite nano-photocatalyst. *Separation and Purification Technology*, *67*(3), 355–363. https://doi.org/10.1016/j.seppur.2009.04.001

Chou, T. P., Zhang, Q., Russo, B., Fryxell, G. E., & Cao, G. (2007). Titania Particle Size Effect on the Overall Performance of Dye-Sensitized Solar Cells. *The Journal of Physical Chemistry C*, *111*(17), 6296–6302. https://doi.org/10.1021/jp068939f

Cuong, N. D., Khieu, D. Q., Hoa, T. T., Quang, D. T., Viet, P. H., Lam, T. D., et al. (2015). Facile synthesis of α-Fe2O3 nanoparticles for high-performance CO gas sensor. *Materials Research Bulletin*, *68*(2), 302–307. https://doi.org/10.1016/j.materresbull.2015.03.069

Dai, X., Lu, G., Hu, Y., Xie, X., Wang, X., & Sun, J. (2019). Reversible redox behavior of Fe2O3/TiO2 composites in the gaseous photodegradation process. *Ceramics International*, *45*(10), 13187–13192. https://doi.org/10.1016/j.ceramint.2019.03.255

Das, B., Mondal, N. K., Bhaumik, R., & Roy, P. (2014). Insight into adsorption equilibrium, kinetics and thermodynamics of lead onto alluvial soil. *International Journal of Environmental Science and Technology*, *11*(4), 1101–1114. https://doi.org/10.1007/s13762-013-0279-z

Dil, E. A., Ghaedi, M., Asfaram, A., Hajati, S., Mehrabi, F., & Goudarzi, A. (2017). Preparation of nanomaterials for the ultrasound-enhanced removal of Pb 2+ ions and malachite green dye: Chemometric optimization and modeling. *Ultrasonics Sonochemistry*, *34*, 677–691. https://doi.org/10.1016/j.ultsonch.2016.07.001

Dil, E. A., Ghaedi, M., Asfaram, A., & Mehrabi, F. (2017). Application of modificated magnetic nanomaterial for optimization of ultrasound-enhanced removal of Pb2+ ions from aqueous solution under experimental design: Investigation of kinetic and isotherm. *Ultrasonics Sonochemistry*, *36*, 409–419. https://doi.org/10.1016/j.ultsonch.2016.12.016

Ding, J., Wei, L., Huang, H., Zhao, Q., Hou, W., Kabutey, F. T., et al. (2018). Tertiary treatment of landfill leachate by an integrated Electro-Oxidation/Electro-Coagulation/Electro-Reduction process: Performance and mechanism. *Journal of Hazardous Materials*, *351*(October 2017), 90–97.

https://doi.org/10.1016/j.jhazmat.2018.02.038

Durães, L., Oliveira, O., Benedini, L., Costa, B. F. O., Matos Beja, A., & Portugal, A. (2011). Sol–gel synthesis of iron(III) oxyhydroxide nanostructured monoliths using Fe(NO3)3·9H2O/CH3CH2OH/NH4OH ternary system. *Journal of Physics and Chemistry of Solids*, *72*(6), 678–684. https://doi.org/10.1016/j.jpcs.2011.02.020

Fatehah, M. O., Aziz, H. A., & Stoll, S. (2014). Stability of ZnO Nanoparticles in Solution. Influence of pH, Dissolution, Aggregation and Disaggregation Effects. *Journal of Colloid Science and Biotechnology*, *3*(1), 75–84. https://doi.org/10.1166/jcsb.2014.1072

Frank, S. N., & Bard, A. J. (1977). Heterogeneous photocatalytic oxidation of cyanide and sulfite in aqueous solutions at semiconductor powders. *The Journal of Physical Chemistry*, *81*(15), 1484–1488. https://doi.org/10.1021/j100530a011

Fu, H., Sun, S., Yang, X., Li, W., An, X., Zhang, H., et al. (2018). A facile coating method to construct uniform porous α-Fe2O3@TiO2 core-shell nanostructures with enhanced solar light photocatalytic activity. *Powder Technology*, *328*, 389–396. https://doi.org/10.1016/j.powtec.2018.01.067

Gallego-Urrea, J. A., Hammes, J., Cornelis, G., & Hassellöv, M. (2016). Coagulation and sedimentation of gold nanoparticles and illite in model natural waters: Influence of initial particle concentration. *NanoImpact*, *3–4*, 67–74. https://doi.org/10.1016/j.impact.2016.10.004

Gaya, U. I., & Abdullah, A. H. (2008). Heterogeneous photocatalytic degradation of organic contaminants over titanium dioxide: A review of fundamentals, progress and problems. *Journal of Photochemistry and Photobiology C: Photochemistry Reviews*, *9*(1), 1–12. https://doi.org/10.1016/j.jphotochemrev.2007.12.003

Gromova, Y. A., Maslov, V. G., Baranov, M. A., Serrano-García, R., Kuznetsova, V. A., Purcell-Milton, F., et al. (2018). Magnetic and Optical Properties of Isolated and Aggregated CoFe2O4 Superparamagnetic Nanoparticles Studied by MCD Spectroscopy. *The Journal of Physical Chemistry C*, *122*(21), 11491–11497. https://doi.org/10.1021/acs.jpcc.8b00829

Habibi, M. H., & Karimi, B. (2014). Application of impregnation combustion method for fabrication of nanostructure CuO/ZnO composite oxide : XRD , FESEM , DRS and FTIR study. *Journal of Industrial and Engineering Chemistry*, *20*(4), 1566–1570. https://doi.org/10.1016/j.jiec.2013.07.048

Han, R., Li, W., Pan, W., Zhu, M., Zhou, D., & Li, F. (2015). 1D Magnetic Materials of Fe3O4 and Fe with High Performance of Microwave Absorption Fabricated by Electrospinning Method. *Scientific Reports*, *4*(1), 7493. https://doi.org/10.1038/srep07493

Herrmann, J.-M. (2010). Fundamentals and misconceptions in photocatalysis. *Journal of Photochemistry and Photobiology A: Chemistry*, *216*(2–3), 85–93. https://doi.org/10.1016/j.jphotochem.2010.05.015

Huang, X., Zhao, G., Wang, G., & Irvine, J. T. S. (2018). Synthesis and applications of nanoporous perovskite metal oxides. *Chemical Science*, *9*(15), 3623–3637. https://doi.org/10.1039/C7SC03920D

Hurum, D. C., Agrios, A. G., Gray, K. A., Rajh, T., & Thurnauer, M. C. (2003). Explaining the Enhanced Photocatalytic Activity of Degussa P25 Mixed-Phase TiO2 Using EPR. *The Journal of Physical Chemistry B*, *107*(19), 4545–4549. https://doi.org/10.1021/jp0273934

Ibhadon, A., & Fitzpatrick, P. (2013). Heterogeneous Photocatalysis: Recent Advances and Applications. *Catalysts*, *3*(1), 189–218. https://doi.org/10.3390/catal3010189

Jain, R., Mathur, M., Sikarwar, S., & Mittal, A. (2007). Removal of the hazardous dye rhodamine B through photocatalytic and adsorption treatments. *Journal of Environmental Management*, *85*(4), 956–964. https://doi.org/10.1016/j.jenvman.2006.11.002

Jalil, A. A., Triwahyono, S., Adam, S. H., Rahim, N. D., Aziz, M. A. A., Hairom, N. H. H., et al. (2010). Adsorption of methyl orange from aqueous solution onto calcined Lapindo volcanic mud. *Journal of Hazardous Materials*, *181*(1–3), 755–762. https://doi.org/10.1016/j.jhazmat.2010.05.078

Jamalluddin, N. A., & Abdullah, A. Z. (2011). Reactive dye degradation by combined Fe(III)/TiO2 catalyst and ultrasonic irradiation: Effect of Fe(III) loading and calcination temperature. *Ultrasonics Sonochemistry*, *18*(2), 669–678. https://doi.org/10.1016/j.ultsonch.2010.09.004

Jin, H., Zhao, X., Wu, Z., Cao, C., & Guo, L. (2017). Supercritical water synthesis of nano-particle catalyst on TiO2 and its application in supercritical water gasification of biomass. *Journal of Experimental Nanoscience*, *12*(1), 72–82. https://doi.org/10.1080/17458080.2016.1262066

Katsou, E., Malamis, S., & Haralambous, K. J. (2011). Industrial wastewater pre-treatment for heavy metal reduction by employing a sorbent-assisted ultrafiltration system. *Chemosphere*, *82*(4), 557–564. https://doi.org/10.1016/j.chemosphere.2010.10.022

Khin, M. M., Nair, A. S., Babu, V. J., Murugan, R., & Ramakrishna, S. (2012). A review on nanomaterials for environmental remediation. *Energy & Environmental Science*, *5*(8), 8075. https://doi.org/10.1039/c2ee21818f

Kho, Y. K., Iwase, A., Teoh, W. Y., Mädler, L., Kudo, A., & Amal, R. (2010). Photocatalytic H2 Evolution over TiO2 Nanoparticles. The Synergistic Effect of Anatase and Rutile. *The Journal of Physical Chemistry C*, *114*(6), 2821–2829. https://doi.org/10.1021/jp910810r

Kılıç, B., Gedik, N., Mucur, S. P., Hergul, A. S., & Gür, E. (2015). Band gap engineering and modifying surface of TiO2 nanostructures by Fe2O3 for enhanced-performance of dye sensitized solar cell. *Materials Science in Semiconductor Processing*, *31*, 363–371. https://doi.org/10.1016/j.mssp.2014.12.020

Konstantinou, I. K., & Albanis, T. A. (2004). TiO2-assisted photocatalytic degradation of azo dyes in aqueous solution: kinetic and mechanistic investigations. *Applied Catalysis B: Environmental*, *49*(1), 1–14. https://doi.org/10.1016/j.apcatb.2003.11.010

Kosmulski, M. (2009). pH-dependent surface charging and points of zero charge. IV. Update and new approach. *Journal of Colloid and Interface Science*, *337*(2), 439–448. https://doi.org/10.1016/j.jcis.2009.04.072

Lachheb, H., Ajala, F., Hamrouni, A., Houas, A., Parrino, F., & Palmisano, L. (2017). Electron transfer in ZnO–Fe2O3 aqueous slurry systems and its effects on visible light photocatalytic activity. *Catalysis Science & Technology*, *7*(18), 4041–4047. https://doi.org/10.1039/C7CY01085K

Lazar, M., Varghese, S., & Nair, S. (2012). Photocatalytic Water Treatment by Titanium Dioxide: Recent Updates. *Catalysts*, *2*(4), 572–601. https://doi.org/10.3390/catal2040572

Li, W., Liu, X., & Li, H. (2015). photocatalytic activity under visible light. *Journal of Materials Chemistry A: Materials for energy and sustainability*, *3*, 15214–15224. https://doi.org/10.1039/C5TA00763A

Li, X., Yu, J., & Jaroniec, M. (2016). Hierarchical photocatalysts. *Chemical Society Reviews*, *45*(9), 2603–2636. https://doi.org/10.1039/C5CS00838G

Lin, C.-I., & Wang, L.-H. (2008). Rate equations and isotherms for two adsorption models. *Journal of the Chinese Institute of Chemical Engineers*, *39*(6), 579–585. https://doi.org/10.1016/j.jcice.2008.04.003

Lin, Y., & Mehrvar, M. (2018). Photocatalytic Treatment of An Actual Confectionery Wastewater Using Ag/TiO2/Fe2O3: Optimization of Photocatalytic Reactions Using Surface Response Methodology. *Catalysts*, *8*(10), 409. https://doi.org/10.3390/catal8100409

Lin, Z., Liu, P., Yan, J., & Yang, G. (2015). Matching energy levels between TiO2 and α-Fe2O3 in a core–shell nanoparticle for visible-light photocatalysis. *Journal of Materials Chemistry A*, *3*(28), 14853–14863. https://doi.org/10.1039/C5TA02958A

Liu, J., He, J., Wang, L., Li, R., Chen, P., Rao, X., et al. (2016). NiO-PTA supported on ZIF-8 as a highly effective catalyst for hydrocracking of Jatropha oil. *Scientific Reports*, *6*(1), 23667. https://doi.org/10.1038/srep23667

Liu, Y., Luo, C., Sun, J., Li, H., Sun, Z., & Yan, S. (2015). Enhanced adsorption removal of methyl orange from aqueous solution by nanostructured proton-containing δ-MnO2. *Journal of Materials Chemistry A*, *3*(10), 5674–5682. https://doi.org/10.1039/C4TA07112C

Macák, J. M., Tsuchiya, H., Ghicov, A., & Schmuki, P. (2005). Dye-sensitized anodic TiO2 nanotubes. *Electrochemistry Communications*, *7*(11), 1133–1137. https://doi.org/10.1016/j.elecom.2005.08.013

Malik, A. S., Letson, D., & Crutchfield, S. R. (1993). Point/Nonpoint Source Trading of Pollution Abatement: Choosing the Right Trading Ratio. *American Journal of Agricultural Economics*, *75*(4), 959. https://doi.org/10.2307/1243983

Mamba, G., & Mishra, A. K. (2016). Graphitic carbon nitride (g-C3N4) nanocomposites: A new and exciting generation of visible light driven photocatalysts for environmental pollution remediation. *Applied Catalysis B: Environmental*, *198*, 347–377. https://doi.org/10.1016/j.apcatb.2016.05.052

Mandelbaum, P. A., Regazzoni, A. E., Blesa, M. A., & Bilmes, S. A. (1999). Photo-Electro-Oxidation of Alcohols on Titanium Dioxide Thin Film Electrodes. *The Journal of*

Physical Chemistry B, *103*(26), 5505–5511. https://doi.org/10.1021/jp984812h

Mendiola-Alvarez, S. Y., Hernández-Ramírez, A., Guzmán-Mar, J. L., Maya-Treviño, M. L., Caballero-Quintero, A., & Hinojosa-Reyes, L. (2019). A novel P-doped Fe2O3-TiO2 mixed oxide: Synthesis, characterization and photocatalytic activity under visible radiation. *Catalysis Today*, *328*(November 2018), 91–98. https://doi.org/10.1016/j.cattod.2019.01.004

Mirmasoomi, S. R., Mehdipour Ghazi, M., & Galedari, M. (2017). Photocatalytic degradation of diazinon under visible light using TiO2/Fe2O3 nanocomposite synthesized by ultrasonic-assisted impregnation method. *Separation and Purification Technology*, *175*, 418–427. https://doi.org/10.1016/j.seppur.2016.11.021

Monárrez-Cordero, B. E., Amézaga-Madrid, P., Sáenz-Trevizo, A., Pizá-Ruiz, P., Antúnez-Flores, W., & Miki-Yoshida, M. (2018). Synthesis and characterization of composite Fe-Ti oxides nanoparticles with high surface area obtained via AACVD. *Ceramics International*, *44*(6), 6990–6996. https://doi.org/10.1016/j.ceramint.2018.01.132

Nguyen, K., Hoa, N. D., Hung, C. M., Thanh Le, D. T., Van Duy, N., & Van Hieu, N. (2018). A comparative study on the electrochemical properties of nanoporous nickel oxide nanowires and nanosheets prepared by a hydrothermal method. *RSC Advances*, *8*(35), 19449–19455. https://doi.org/10.1039/C8RA02862A

Ning, B., Graham, N., Zhang, Y., Nakonechny, M., & Gamal El-Din, M. (2007). Degradation of Endocrine Disrupting Chemicals by Ozone/AOPs. *Ozone: Science & Engineering*, *29*(3), 153–176. https://doi.org/10.1080/01919510701200012

Ofomaja, A. E., Unuabonah, E. I., & Oladoja, N. A. (2010). Competitive modeling for the biosorptive removal of copper and lead ions from aqueous solution by Mansonia wood sawdust. *Bioresource Technology*, *101*(11), 3844–3852. https://doi.org/10.1016/j.biortech.2009.10.064

Ohtani, B. (2010). Photocatalysis A to Z—What we know and what we do not know in a scientific sense. *Journal of Photochemistry and Photobiology C: Photochemistry Reviews*, *11*(4), 157–178. https://doi.org/10.1016/j.jphotochemrev.2011.02.001

Papic, S. (2004). Removal of some reactive dyes from synthetic wastewater by combined Al(III) coagulation/carbon adsorption process. *Dyes and Pigments*, *62*(3), 291–298. https://doi.org/10.1016/S0143-7208(03)00148-7

Porter, I. J., Cushing, S. K., Carneiro, L. M., Lee, A., Ondry, J. C., Dahl, J. C., et al. (2018). Photoexcited Small Polaron Formation in Goethite (α-FeOOH) Nanorods Probed by Transient Extreme Ultraviolet Spectroscopy. *The Journal of Physical Chemistry Letters*, *9*(14), 4120–4124. https://doi.org/10.1021/acs.jpclett.8b01525

Pype, M., Lawrence, M. G., Keller, J., & Gernjak, W. (2016). Reverse osmosis integrity monitoring in water reuse: The challenge to verify virus removal – A review. *Water Research*, *98*, 384–395. https://doi.org/10.1016/j.watres.2016.04.040

Qamar, M. T., Aslam, M., Ismail, I. M. I., Salah, N., & Hameed, A. (2015). Synthesis, Characterization, and Sunlight Mediated Photocatalytic Activity of CuO Coated ZnO for the Removal of Nitrophenols. *ACS Applied Materials & Interfaces*, *7*(16), 8757–8769. https://doi.org/10.1021/acsami.5b01273

Rather, L. J., Jameel, S., Dar, O. A., Ganie, S. A., Bhat, K. A., & Mohammad, F. (2019). Advances in the sustainable technologies for water conservation in textile industries. In *Water in Textiles and Fashion* (pp. 175–194). Elsevier. https://doi.org/10.1016/B978-0-08-102633-5.00010-5

Rivera, J. M., Rincón, S., Ben Youssef, C., & Zepeda, A. (2016). Highly Efficient Adsorption of Aqueous Pb(II) with Mesoporous Metal-Organic Framework-5: An Equilibrium and Kinetic Study. *Journal of Nanomaterials*, *2016*, 1–9. https://doi.org/10.1155/2016/8095737

Rostami, M., Aghajanzadeh, M., Zamani, M., Manjili, H. K., & Danafar, H. (2018). Sono-chemical synthesis and characterization of Fe3O4@mTiO2-GO nanocarriers for dual-targeted colon drug delivery. *Research on Chemical Intermediates*, *44*(3), 1889–1904. https://doi.org/10.1007/s11164-017-3204-0

Saha, N., Sarkar, A., Ghosh, A. B., Dutta, A. K., Bhadu, G. R., Paul, P., & Adhikary, B. (2015). Highly active spherical amorphous MoS 2 : facile synthesis and application in photocatalytic degradation of rose bengal dye and hydrogenation of nitroarenes. *RSC Advances*, *5*(108), 88848–88856. https://doi.org/10.1039/C5RA19442C

Saravanan, R., Aviles, J., Gracia, F., Mosquera, E., & Gupta, V. K. (2018). Crystallinity and lowering band gap induced visible light photocatalytic activity of TiO2/CS (Chitosan) nanocomposites. *International Journal of Biological Macromolecules*, *109*, 1239–1245. https://doi.org/10.1016/j.ijbiomac.2017.11.125

Sharma, B., Boruah, P. K., Yadav, A., & Das, M. R. (2018). TiO2–Fe2O3 nanocomposite heterojunction for superior charge separation and the photocatalytic inactivation of pathogenic bacteria in water under direct sunlight irradiation. *Journal of Environmental Chemical Engineering*, *6*(1), 134–145. https://doi.org/10.1016/j.jece.2017.11.025

Shojaie, A., Fattahi, M., Jorfi, S., & Ghasemi, B. (2018). Synthesis and evaluations of - Fe3O4–TiO2–Ag nanocomposites for photocatalytic degradation of 4 - chlorophenol (4 - CP): effect of Ag and Fe compositions. *International Journal of Industrial Chemistry*, (0123456789), 24–26.

Sigoli, F. A., Davolos, M. R., & Jafelicci, M. (1997). Morphological evolution of zinc oxide originating from zinc hydroxide carbonate. *Journal of Alloys and Compounds*, *262–263*, 292–295. https://doi.org/10.1016/S0925-8388(97)00404-0

Singh, J., Sharma, S., Aanchal, & Basu, S. (2019). Synthesis of Fe2O3/TiO2 monoliths for the enhanced degradation of industrial dye and pesticide via photo-Fenton catalysis. *Journal of Photochemistry and Photobiology A: Chemistry*, *376*(February), 32–42. https://doi.org/10.1016/j.jphotochem.2019.03.004

Stock, N. L., Peller, J., Vinodgopal, K., & Kamat, P. V. (2000). Combinative Sonolysis and Photocatalysis for Textile Dye Degradation. *Environmental Science & Technology*, *34*(9), 1747–1750. https://doi.org/10.1021/es991231c

Subramonian, W., Wu, T. Y., & Chai, S. (2017a). Using one-step facile and solvent-free mechanochemical process to synthesize photoactive Fe2O3-TiO2 for treating industrial wastewater. *Journal of Alloys and Compounds*, *695*, 496–507. https://doi.org/10.1016/j.jallcom.2016.10.006

Subramonian, W., Wu, T. Y., & Chai, S. (2017b). Photocatalytic degradation of industrial pulp and paper mill effluent using synthesized magnetic Fe2O3-TiO2 : Treatment efficiency and characterizations of reused photocatalyst. *Journal of Environmental Management*, *187*, 298–310. https://doi.org/10.1016/j.jenvman.2016.10.024

Sui, Y., Liu, Q., Jiang, T., & Guo, Y. (2018). Synthesis of nano-TiO2 photocatalysts with tunable Fe doping concentration from Ti-bearing tailings. *Applied Surface Science*, *428*, 1149–1158. https://doi.org/10.1016/j.apsusc.2017.09.197

Sun, B., Zhou, W., Li, H., Ren, L., Qiao, P., Xiao, F., et al. (2018). Magnetic Fe2O3/mesoporous black TiO2 hollow sphere heterojunctions with wide-spectrum response and magnetic separation. *Applied Catalysis B: Environmental*, *221*(July 2017), 235–242. https://doi.org/10.1016/j.apcatb.2017.09.023

Tang, X., Zheng, H., Teng, H., Sun, Y., Guo, J., Xie, W., et al. (2016). Chemical coagulation process for the removal of heavy metals from water: a review. *Desalination and Water Treatment*, *57*(4), 1733–1748. https://doi.org/10.1080/19443994.2014.977959

Valero-Romero, M. J., Santaclara, J. G., Oar-Arteta, L., van Koppen, L., Osadchii, D. Y., Gascon, J., & Kapteijn, F. (2019). Photocatalytic properties of TiO2 and Fe-doped TiO2 prepared by metal organic framework-mediated synthesis. *Chemical Engineering Journal*, *360*(November 2018), 75–88. https://doi.org/10.1016/j.cej.2018.11.132

Wahyuningsih, S., Ramelan, A. H., Prasetyawati, L., Saputri, L. N. M. Z., Ichsan, S., & Kristiawan, Y. R. (2018). The Influence of Fe2O3 Addition on the TiO2 Structure and Photoactivity Properties. *IOP Conference Series: Materials Science and Engineering*, *333*, 012033. https://doi.org/10.1088/1757-899X/333/1/012033

Wang, D. K., Elma, M., Motuzas, J., Hou, W., Xie, F., & Zhang, X. (2017). Rational design and synthesis of molecular-sieving, photocatalytic, hollow fiber membranes for advanced water treatment applications. *Journal of Membrane Science*, *524*(September 2016), 163–173. https://doi.org/10.1016/j.memsci.2016.10.052

Wang, D., Wang, Y., Li, X., Luo, Q., An, J., & Yue, J. (2008). Sunlight photocatalytic activity of polypyrrole–TiO2 nanocomposites prepared by ‘in situ’ method. *Catalysis Communications*, *9*(6), 1162–1166. https://doi.org/10.1016/j.catcom.2007.10.027

Wang, T., Yang, G., Liu, J., Yang, B., Ding, S., Yan, Z., & Xiao, T. (2014). Orthogonal synthesis, structural characteristics, and enhanced visible-light photocatalysis of mesoporous Fe2O3/TiO2 heterostructured microspheres. *Applied Surface Science*, *311*, 314–323. https://doi.org/10.1016/j.apsusc.2014.05.060

Wang, Y., Li, L., Huang, X., Li, Q., & Li, G. (2015). New insights into fluorinated TiO2 (brookite, anatase and rutile) nanoparticles as efficient photocatalytic redox catalysts. *RSC Advances*, *5*(43), 34302–34313. https://doi.org/10.1039/C4RA17076H

Wang, Zeyan, Liu, Y., Huang, B., Dai, Y., Lou, Z., Wang, G., et al. (2014). Progress on extending the light absorption spectra of photocatalysts. *Physical Chemistry Chemical Physics*, *16*(7), 2758. https://doi.org/10.1039/c3cp53817f

Wang, Zuohua, Xiang, B., Cheng, R., & Li, Y. (2010). Behaviors and mechanism of acid dyes sorption onto diethylenetriamine-modified native and enzymatic hydrolysis starch. *Journal of Hazardous Materials*, *183*(1–3), 224–232.

https://doi.org/10.1016/j.jhazmat.2010.07.015

Wu, L., Yan, H., Xiao, J., Li, X., Wang, X., & Zhao, T. (2017). Characterization and photocatalytic properties of nano-Fe2O3–TiO2 composites prepared through the gaseous detonation method. *Ceramics International*, *43*(16), 14334–14339. https://doi.org/10.1016/j.ceramint.2017.07.189

Yang, H., Masse, S., Rouelle, M., Aubry, E., Li, Y., Roux, C., et al. (2015). Magnetically recoverable iron oxide–hydroxyapatite nanocomposites for lead removal. *International Journal of Environmental Science and Technology*, *12*(4), 1173–1182. https://doi.org/10.1007/s13762-014-0514-2

Yang, Y., Yan, B., & Shen, W. (2010). Assessment of point and nonpoint sources pollution in Songhua River Basin, Northeast China by using revised water quality model. *Chinese Geographical Science*, *20*(1), 30–36. https://doi.org/10.1007/s11769-010-0030-3

Zhang, W., Zhang, S., Wang, J., Wang, M., He, Q., Song, J., et al. (2018). Hybrid functionalized chitosan-Al2O3@SiO2 composite for enhanced Cr(VI) adsorption. *Chemosphere*, *203*, 188–198. https://doi.org/10.1016/j.chemosphere.2018.03.188

Zhou, L., Pan, S., Chen, X., Zhao, Y., Zou, B., & Jin, M. (2014). Kinetics and thermodynamics studies of pentachlorophenol adsorption on covalently functionalized Fe3O4@SiO2–MWCNTs core–shell magnetic microspheres. *Chemical Engineering Journal*, *257*, 10–19. https://doi.org/10.1016/j.cej.2014.07.060